doi:10.1093/plcell/koaa035

THE PLANT CELL

THE PLANT CELL 2021: 33: 642–670

Research Article

Plasma membrane nano-organization specifies phosphoinositide effects on Rho-GTPases and actin dynamics in tobacco pollen tubes

Marta Fratini [1,†], Praveen Krishnamoorthy [1,†,§], Irene Stenzel [1], Mara Riechmann [1,‖], Monique Matzner [1], Kirsten Bacia [2], Mareike Heilmann [1] and Ingo Heilmann [1,*,‡]

1 Department of Plant Biochemistry, Institute of Biochemistry and Biotechnology, Martin-Luther-University Halle-Wittenberg, Halle (Saale), Germany
2 Department of Biophysical Chemistry, Institute of Chemistry, Martin-Luther-University Halle-Wittenberg, Halle (Saale), Germany

*Author for correspondence: ingo.heilmann@biochemtech.uni-halle.de (I.H.).
†These authors contributed equally to this work (M.F., P.K.).
‡Senior author.
§Present address: Washington University Center for Cellular Imaging (WUCCI), Washington University in St. Louis, St. Louis, MO, USA.
‖Present address: Molecular Cell Biology and Transgenic Research, Institute of Biochemistry, Christian-Albrechts-University Kiel, Germany.

M.F., P.K., I.S., M.R., M.M., and M.H. performed the experiments; M.F., P.K., I.S., M.M., M.H., K.B., and I.H. analyzed the data; M.F., P.K., and I.H. designed the research; I.H. wrote the manuscript.

The author responsible for distribution of materials integral to the findings presented in this article in accordance with the policy described in the Instructions for Authors (https://academic.oup.com/plcell/pages/General-Instructions) is: Ingo Heilmann (ingo.heilmann@biochemtech.uni-halle.de).

Abstract

Pollen tube growth requires coordination of cytoskeletal dynamics and apical secretion. The regulatory phospholipid phosphatidylinositol 4,5-bisphosphate (PtdIns(4,5)P_2) is enriched in the subapical plasma membrane of pollen tubes of *Arabidopsis thaliana* and tobacco (*Nicotiana tabacum*) and can influence both actin dynamics and secretion. How alternative PtdIns(4,5)P_2 effects are specified is unclear. In tobacco pollen tubes, spinning disc microscopy (SD) reveals dual distribution of a fluorescent PtdIns(4,5)P_2-reporter in dynamic plasma membrane nanodomains vs. apparent diffuse membrane labeling, consistent with spatially distinct coexisting pools of PtdIns(4,5)P_2. Several PI4P 5-kinases (PIP5Ks) can generate PtdIns(4,5)P_2 in pollen tubes. Despite localizing to one membrane region, the PIP5Ks AtPIP5K2-EYFP and NtPIP5K6-EYFP display distinctive overexpression effects on cell morphologies, respectively related to altered actin dynamics or membrane trafficking. When analyzed by SD, AtPIP5K2-EYFP associated with nanodomains, whereas NtPIP5K6-EYFP localized diffusely. Chimeric AtPIP5K2-EYFP and NtPIP5K6-EYFP variants with reciprocally swapped membrane-associating domains evoked reciprocally shifted effects on cell morphology upon overexpression. Overall, active PI4P 5-kinase variants stabilized actin when targeted to nanodomains, suggesting a role of nanodomain-associated PtdIns(4,5)P_2 in actin regulation. This notion is further supported by interaction and proximity of nanodomain-associated AtPIP5K2 with the Rho-GTPase NtRac5, and by its functional interplay with elements of Rho of plants signaling. Plasma membrane nano-organization may thus aid the specification of PtdIns(4,5)P_2 functions to coordinate cytoskeletal dynamics and secretion.

Received August 12, 2020. Accepted November 23, 2020. Advance access publication December 18, 2020

IN A NUTSHELL

Background: Each living cell is surrounded by a plasma membrane, which is composed of lipids that form a hydrophobic barrier. Certain membrane lipids help control biological processes at the plasma membrane, and we demonstrate that such regulatory lipids form dot-like patterns, which guide certain physiological processes and thereby contribute to the control of overall cellular physiology. The larger cellular picture emerging from the dot-like lipid patterns is somewhat reminiscent of pointillism. Pointillism is a painting technique first developed by G. Seurat and P. Signac in 1886. The technique uses a multitude of tiny dots well-positioned all over a canvas to create a scene at a much larger-scale. When we look at the overall painting, all the dots together generate a well-defined image. However, once we look closer we can still appreciate the individual dots. Regulatory lipids in cellular membranes can also be visualized by fluorescence labeling as tiny colorful dots; by using advanced microscopy techniques the lipids are found in different patterns or in different areas. Similar to pointillism paintings, where many dots together generate a specific shape (a tree, a boat, or a face), the positions of regulatory lipids in a membrane enable coordinated physiological functions according to the patterns they create.

Question: We address how signaling lipids form patterns, how their distribution is regulated and which cellular functions they control.

Findings: We studied tobacco (*N. tabacum*) pollen tubes whose shape relies strictly on the correct positioning of signaling lipids. We show that the important regulatory lipid phosphatidylinositol-4,5-bisphosphate (PIP_2), localizes in plasma membrane dots ("nanodomains") at the tip of pollen tubes where the cells expand. PIP_2 localization in nanodomains depends on the lipid kinase PIP5K2, which also localizes in nanodomains. Both PIP_2 and PIP5K2 nanodomains are dynamic and control cytoskeletal dynamics in pollen tubes.

Next steps: In the future, we aim to understand how the cytoskeleton, lipid kinases and PIP_2 act together in the tip of pollen tubes and also in different other types of plant cells. We furthermore aim to elucidate the molecular mechanisms by which plasma membrane nanodomains are formed, maintained and dynamically disassembled.

Introduction

The extreme cell shapes of plant pollen tubes or root hairs arise from polar tip growth (Hepler and Winship, 2015; Orr et al., 2020). For polar tip growth, polarized cell expansion is achieved by the tip-focused transport of vesicles containing cell wall material and membrane towards the expanding cell apex, their secretion at a narrow area of the cell surface and—upon cargo delivery—the endocytotic retrieval of a majority of vesicles for recycling (Cheung and Wu, 2008). The balance of apical secretion and recycling of vesicles requires the coordination of membrane trafficking and cytoskeletal dynamics at the plasma membrane (Grebnev et al., 2017; Guo and Yang, 2020; Orr et al., 2020).

The plasma membrane serves multiple physiological functions, including as a hydrophobic barrier, for selective transport, signal transduction, attachment of the cytoskeleton and for membrane trafficking. Its body is composed of amphiphilic lipids, including glycerophospholipids, sphingolipids, and sterols (Furt et al., 2011; Mamode Cassim et al., 2019). Some lipid classes are highly abundant, such as the structural glycerophospholipids, phosphatidylcholine, or phosphatidylethanolamine, whereas other lipid classes occur in much smaller proportions, such as phosphatidylserine or other anionic lipids, such as phosphoinositides (Furt et al., 2011), which are in the focus of this study. Phosphoinositides are a minor class of regulatory phospholipids that derive from phosphatidylinositol by the phosphorylation of the inositol head group and in eukaryotes contribute to the control of membrane trafficking and cytoskeletal dynamics (Heilmann and Heilmann, 2015). Importantly, phosphoinositides can bind different protein partners at the cytosolic face of the plasma membrane (Heilmann, 2016; Gerth et al., 2017b; Noack and Jaillais, 2020), thereby influencing alternative processes. It is an important unresolved question of eukaryotic cell biology how phosphoinositides exert specific regulatory effects.

A role of phosphoinositides in the control of polar tip growth has been reported by numerous studies on root hairs (Vincent et al., 2005; Kusano et al., 2008; Stenzel et al., 2008; Stanislas et al., 2015) or pollen tubes (Kost et al., 1999; Monteiro et al., 2005a, 2005b; Ischebeck et al., 2008; Kost, 2008; Sousa et al., 2008; Ischebeck et al., 2010a, 2010b, 2011; Stenzel et al., 2012; Heilmann and Heilmann, 2015; Bloch et al., 2016); or moss filaments (Saavedra et al., 2011, 2015); or even fungal hyphae (Ischebeck et al., 2010a; Mähs et al., 2012). While phosphoinositides evidently contribute to the control and coordination of various aspects of polar tip growth in plants, the factors determining their individual specific effects have remained elusive.

The subcellular distribution of some phosphoinositides has been visualized in plant cells by genetically encoded fluorescent reporters, such as those based on the Pleckstrin homology (PH)-domain of mammalian phospholipase C (PLC)δ1 that specifically recognize phosphatidylinositol 4,5-bisphosphate ($PtdIns(4,5)P_2$; Varnai and Balla, 1998; Kost et al., 1999; Balla and Varnai, 2002; van Leeuwen et al., 2007; Simon et al., 2014) or other lipid-binding modules specific for phosphatidylinositol 4-phosphate (PtdIns4P) (Vermeer

et al., 2009; Simon et al., 2014, 2016). In pollen tubes, fluorescent biosensors show PtdIns(4,5)P_2 enriched in a subapical plasma membrane region (Kost et al., 1999), where the lipid has been proposed to influence both membrane trafficking and cytoskeletal dynamics (Malho et al., 2006; Kost, 2008; Ischebeck et al., 2010a; Heilmann and Heilmann, 2015; Gerth et al., 2017b). The PtdIns(4,5)P_2-rich region of the subapical plasma membrane covers from approx. 1–13 µm as measured from the tip of growing tobacco (*Nicotaniana tabacum*) pollen tubes, spanning a region accumulating secretory and recycling vesicles that is characterized by a fine-tuned actin network required for proper trafficking (Hepler and Winship, 2015; Heilmann and Ischebeck, 2016; Grebnev et al., 2017).

PtdIns(4,5)P_2 in this region of the pollen tube plasma membrane is essential for polar tip-growth, and genetic lesions in PtdIns(4,5)P_2 biosynthesis result in massively decreased pollen germination and in impaired pollen tube expansion (Ischebeck et al., 2008; Sousa et al., 2008; Heilmann and Ischebeck, 2016). As loss of function mutants show defects in pollen germination, regulatory effects of PtdIns(4,5)P_2 have been assessed mostly by gain of function approaches, in which the perturbation of PtdIns(4,5)P_2 biosynthesis also results in defective polar tip growth. At least two categories of characteristic aberrant cell morphologies arise from the overexpression of different PI4P 5-kinases in pollen tubes. For instance, the overexpression of the Arabidopsis PI4P 5-kinases AtPIP5K4 (Ischebeck et al., 2008, 2010b; Sousa et al., 2008), AtPIP5K5 (Ischebeck et al., 2008, 2010b), AtPIP5K6 (Zhao et al., 2010), or tobacco NtPIP5K6 (Stenzel et al., 2012) results in a characteristic and irregular tip branching phenotype of the pollen tubes, which is accompanied by increased apical deposition of pectin. The associated cell morphologies have previously been summarized as "secretion phenotypes" (Ischebeck et al., 2010b). By contrast, these effects are not apparent when other PI4P 5-kinases are overexpressed, such as AtPIP5K2 (Stenzel et al., 2012), AtPIP5K10 (Ischebeck et al., 2011) or AtPIP5K11 (Ischebeck et al., 2011), which instead cause extensive pollen tube tip swelling upon overexpression, proposed to be linked to changes in the actin cytoskeleton (Ischebeck et al., 2011). It is important to note that no increased pectin deposition or tip branching is observed upon the overexpression of AtPIP5K2, AtPIP5K10, and AtPIP5K11 (Ischebeck et al., 2011; Stenzel et al., 2012), suggesting that these enzymes are functionally divergent (Stenzel et al., 2012).

The differences in reported effects of PI4P 5-kinases on cell morphology make the pollen tube a unique model to study the determinants for the specificity of PtdIns(4,5)P_2 effects within a well-defined plasma membrane region of one cell (Ischebeck et al., 2010a; Stenzel et al., 2012; Heilmann and Heilmann, 2015; Gerth et al., 2017b). As catalytic activity of PI4P 5-kinases was required to mediate the respective effects on cell morphologies (Ischebeck et al., 2008, 2011; Stenzel et al., 2012), we have previously proposed the presence of at least two functional pools of PtdIns(4,5)P_2 within the subapical plasma membrane of pollen tube cells (Ischebeck et al., 2011; Stenzel et al., 2012; Heilmann and Heilmann, 2013, 2015; Heilmann, 2016; Gerth et al., 2017b), which may be defined by the respective PI4P 5-kinases mediating their biosynthesis. Such PtdIns(4,5)P_2 pools may preferentially influence membrane trafficking or cytoskeletal dynamics, respectively (Stenzel et al., 2012). However, direct experimental evidence for or against the pool hypothesis has been elusive so far, and no systematic study has been conducted to compare pollen PI4P 5-kinases to address their proposed distinct functionalities side-by-side.

In *Arabidopsis thaliana*, PI4P 5-kinases are represented as an enzyme family of 11 members (Supplemental Figure 1; Supplemental Data Set 1), which can be divided into subfamilies A (PIP5K10 and PIP5K11) and B (PIP5K1–PIP5K9), based on differences in protein architecture. All isoforms preferentially convert the substrate phosphatidylinositol 4-phosphate (PtdIns4P) to PtdIns(4,5)P_2 in vitro (Ischebeck et al., 2008, 2011, 2013; Stenzel et al., 2008, 2012). Enzymes of subfamily A lack several N-terminal domains found in their counterparts of subfamily B (Figure 1A) and have so far only been found in Arabidopsis. PI4P 5-kinases of subfamily A are only weakly expressed and Arabidopsis *pip5k10 pip5k11* double mutants displayed only minor defects in pollen tube growth (Ischebeck et al., 2011). Overall, the physiological relevance of the "small" PI4P 5-kinases of subfamily A remains thus unclear. By contrast, Arabidopsis mutants with defects in genes for PI4P 5-kinases of subfamily B display massively reduced pollen germination and reduced pollen tube growth, such as reported for the Arabidopsis *pip5k4 pip5k5* mutant (Ischebeck et al., 2008; Sousa et al., 2008), highlighting a pronounced contribution to pollen tube growth. Importantly, pollen-expressed members of the PI4P 5-kinase subfamily B have previously been found to mediate distinct effects either on membrane trafficking, such as AtPIP5K4 and AtPIP5K5 (Ischebeck et al., 2008; Sousa et al., 2008), AtPIP5K6 (Zhao et al., 2010) or NtPIP5K6 (Stenzel et al., 2012), or on the cytoskeleton, such as AtPIP5K2 (Stenzel et al., 2012), raising the question of how PI4P 5-kinases of subfamily B exert isoform-specific regulatory effects.

Among PI4P 5-kinases across kingdoms, the members of the Arabidopsis subfamily B share a unique domain structure consisting of an N-terminal domain, a membrane occupation and recognition nexus repeat domain, a hypervariable linker (Lin)-domain and a catalytic (Cat) domain, which holds a variable insert region (Figure 1A). This domain structure is only found in PI4P 5-kinases of plant origin and not in enzymes from nonplant organisms (Mueller-Roeber and Pical, 2002; Gerth et al., 2017b). The well-defined domain architecture of PI4P 5-kinases of subfamily B enables the comparative analysis of features mediating isoform-specific functionality of the enzymes. To this end, previous work has focused on the comparison of the enzymes

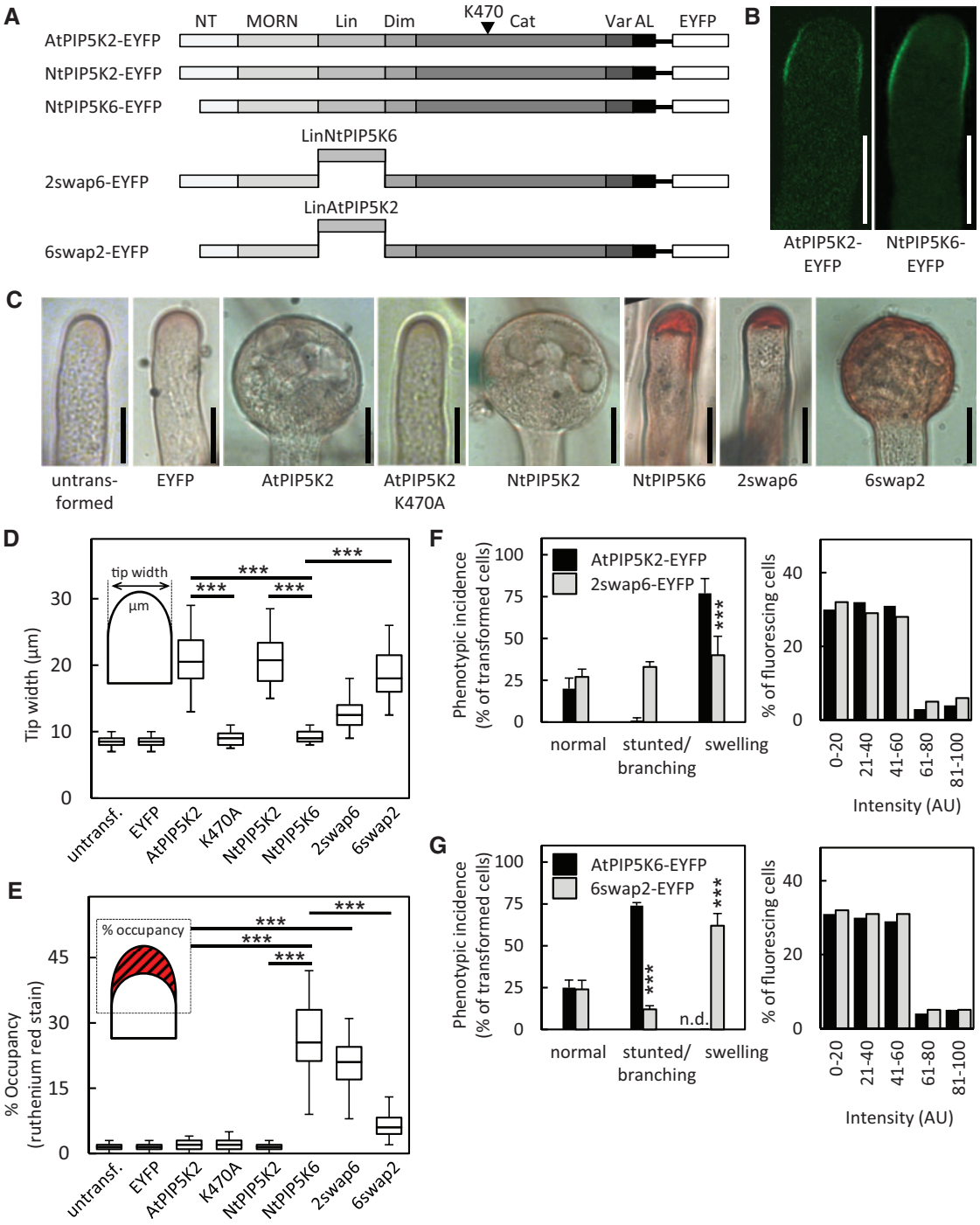

Figure 1 The PI4P 5-kinases AtPIP5K2 and NtPIP5K6 have divergent regulatory effects in tobacco pollen tubes. A, AtPIP5K2, its putative tobacco ortholog NtPIP5K2 and NtPIP5K6 display the characteristic domain structure of PI4P 5-kinases of subfamily B. NT, N-terminal domain; MORN, membrane occupation and recognition nexus-repeat domain; Lin, linker domain; Dim, dimerization domain; Cat, catalytic domain; Var, variable insert domain; AL, activation loop. The chimeric enzymes 2swap6 and 6swap2 were created by reciprocally swapping the Lin-domains between AtPIP5K2 and NtPIP5K6, as indicated. EYFP, yellow fluorescent protein. Arrowhead, position of the catalytic lysine 470 in AtPIP5K2. B, AtPIP5K2-EYFP or NtPIP5K6-EYFP were transiently expressed in tobacco pollen tubes under the control of the Lat52-promoter, and the fluorescence distribution was recorded by confocal microscopy. Representative images show both enzymes localized to a subapical region of the plasma membrane of growing pollen tubes. Scale bar, 10 µm. C, The effects of strongly expressing AtPIP5K2-EYFP, the catalytically inactive variant AtPIP5K2 K470A-EYFP, NtPIP5K2, NtPIP5K6 or the chimeric variants 2swap6-EYFP or 6swap2-EYFP on the morphology of tobacco pollen tubes was assessed upon transient expression under the control of the Lat52 promoter. Representative cell morphologies are shown in comparison to untransformed cells or to pollen tubes expressing an EYFP control, as indicated, and include pollen tube tip swelling or the increased apical deposition of pectin, as stained by ruthenium red. Please note that all pollen tubes shown were stained for equal periods with ruthenium red. Pollen tubes displaying increased apical pectin deposition also showed stunted or branched growth. Scale bars, 10 µm. D, E, The degree of pollen tube tip swelling (D) or of

AtPIP5K2 and NtPIP5K6, which upon overexpression display most pronounced functional differences and mutually exclusive effects on pollen tube morphologies: AtPIP5K2 causes pollen tube tip swelling, whereas NtPIP5K6 evokes pronounced "secretion phenotypes" (Stenzel et al., 2012). To rationalize the functional divergence of AtPIP5K2 and NtPIP5K6, previous analyses have focused on the hypervariable Lin-domains, which contribute to the plasma membrane association of PI4P 5-kinases (Stenzel et al., 2012). Lin-domains are not conserved in sequence between PI4P 5-kinase isoforms, making them ideal candidate regions to mediate isoform-specific membrane recruitment (Stenzel et al., 2012; Heilmann and Heilmann, 2013; Gerth et al., 2017b). The functionality of the Lin-domains is not understood in mechanistic detail, and the regions are predicted to be in part intrinsically disordered. Among PI4P 5-kinases of subfamily B, the functional distinction of AtPIP5K2 has previously been attributed to an increased accumulation of point mutations within the coding region for its Lin-domain, suggesting that the divergent evolution of membrane attachment regions might contribute to the rise of novel functionalities (Stenzel et al., 2012). When Lin-domains were previously swapped between AtPIP5K2 and NtPIP5K6, the exchange resulted in the reciprocal shift in the respectively arising cell morphologies (Stenzel et al., 2012). The combined observations suggest that one reason for the alternative physiological effects of the enzymes was recruitment by their Lin-domains into alternative regulatory contexts at the plasma membrane (Stenzel et al., 2012; Heilmann and Heilmann, 2013).

Different functional aspects of the plasma membrane are defined by the presence of certain protein complexes, resulting in a dynamic landscape of areas with regionally defined functional specifications (Jaillais and Ott, 2020). It is our working hypothesis that the recruitment of PI4P 5-kinases into one or another protein complex at the plasma membrane underlies the functional specificity of PtdIns(4,5)P_2 formed by a given enzyme. Reciprocally, the localized formation of PtdIns(4,5)P_2 may underlie the recruitment of proteins constituting a certain functional environment, possibly resulting in the self-organization of membrane nanodomains with specific functions. Numerous membrane-associated protein complexes mediate their function not diffusely in the plane of the membrane, but are focused in narrow spots (nanodomains, foci) of < 1 µm in diameter, which can be observed by spinning disc microscopy (SD). Examples include the assembly of the EXOCYST complex during secretion (Li et al., 2013; Zhang et al., 2013; Kalmbach et al., 2017; Sekereš et al., 2017) or the recruitment of adaptor proteins and the assembly of the clathrin coat during endocytosis (Konopka et al., 2008; Gadeyne et al., 2014; Bashline et al., 2015; Johnson and Vert, 2017). Similarly, monomeric GTPases of the Rho of plants (ROP) family, which are involved in the coordination of the actin cytoskeleton with secretion and endocytosis (Kost et al., 1999; Kost, 2008; Lee et al., 2008; Yalovsky et al., 2008; Grebnev et al., 2017), distribute into plasma membrane nanodomains (Platre et al., 2019). Interestingly, the overexpression of the tobacco ROP, NtRac5 (tobacco Ras-related C3 botulinum toxin substrate 5), results in actin stabilization and pollen tube tip swelling (Klahre et al., 2006), suggesting a link between phosphoinositides and actin dynamics involving ROPs.

Despite a wealth of information on protein nanodomain patterns and on protein–protein interactions within relevant protein complexes, the contribution of membrane lipids to the formation of particular membrane nanodomains has only recently begun to be unravelled (Platre et al., 2019). So far, there is only limited information on the lateral distribution of phospholipids within the plane of the plasma membrane in plants. In petunia (*Petunia inflata*) pollen tubes, a fluorescence-tagged oxysterol-binding protein decorated a spot-like pattern at the apical plasma membrane (Skirpan et al., 2006). Based on circumstantial evidence, the presence of PtdIns(4,5)P_2-containing membrane nanodomains of ~70 nm in diameter has previously been suggested for plasma membrane vesicles isolated from tobacco leaves (Furt et al., 2010). So far, however, it has remained unclear whether and how PtdIns(4,5)P_2 nanodomains might be formed in living cells, and what their biological functions might be.

Here, we hypothesize that spatial separation of PtdIns(4,5)P_2 in membrane nanodomains might be a reason for the functional divergence of PtdIns(4,5)P_2 formed by different PI4P 5-kinase isoforms in pollen tubes. We show by in vivo SD analysis that within the subapical plasma membrane of tobacco pollen tubes PtdIns(4,5)P_2 occurs both in membrane nanodomains and in a diffuse distribution, suggesting spatially separated coexisting pools of the lipid. We further show that the functionally divergent PI4P 5-kinases AtPIP5K2 and its putative tobacco ortholog NtPIP5K2 associate with plasma membrane nanodomains, whereas canonical NtPIP5K6 does not, and that nanodomain association of PIP5K2 orthologs is required for their divergent function as regulators of ROP signaling and the dynamic actin cytoskeleton.

Figure 1 (Continued)
ruthenium red staining (E) was quantified by measuring tip width ($n \geqslant 200$) or the apical dye occupancy ($n \geqslant 200$), respectively, as indicated. For the box plots, quartiles were first defined by numerically ordering the recorded values. The median divides the number of values in two halves, which are each further divided into quartiles. The ends of the box represent the upper and lower quartiles of recorded values, so the box spans the interquartile range. The median of all recorded values is marked by a horizontal line inside the box. The whiskers extend to the highest and lowest recorded values. F, G, The incidence of stunted growth/branching or tip swelling was recorded in tobacco (*N. tabacum*) pollen tubes upon the strong expression of AtPIP5K2-EYFP or 2swap6-EYFP (F), or upon the strong expression of NtPIP5K6-EYFP or 6swap2-EYFP (G), respectively ($n \geqslant 200$ for all constructs analyzed). Right panels, fluorescence intensity distribution corresponding to the overexpression of the parental (black bars) or chimeric (grey bars) enzymes. The expression of all fusions was driven by the Lat52 promoter. Data are given as means ± standard deviation. Asterisks indicate a significant difference to the control, as indicated, according to a Student's *t* test. ***$P \leqslant 0.001$.

Results

This study is aimed at understanding alternative effects of the regulatory phospholipid, PtdIns(4,5)P_2, on processes relevant to polar tip growth, such as membrane trafficking and actin dynamics. To illustrate previously postulated alternative functions of PI4P 5-kinase isoforms within the subapical plasma membrane of pollen tubes, we performed a systematic side-by-side comparison of phenotypic effects of overexpressing the functionally divergent pollen expressed PI4P 5-kinases, AtPIP5K2/NtPIP5K2 and NtPIP5K6.

The PI4P 5-kinases AtPIP5K2 and NtPIP5K6 exert different regulatory effects in tobacco pollen tubes

AtPIP5K2, NtPIP5K2, and NtPIP5K6 are members of PI4P 5-kinase subfamily B and share a common domain architecture (Figure 1A). Besides these enzymes, our functional comparison also included chimeric enzyme variants of AtPIP5K2 and NtPIP5K6 representing reciprocal swaps of Lin-domains, termed 2swap6 and 6swap2, as indicated in Figure 1A. In growing tobacco pollen tubes, fluorescence-tagged fusions of AtPIP5K2 and NtPIP5K6 localized to the subapical plasma membrane (Figure 1B), as previously reported for the parental enzymes and also for the chimeric variants (Stenzel et al., 2012). Please note that morphologically unaltered pollen tubes as shown in Figure 1B were only obtained upon very low expression levels, as in previous experiments (Stenzel et al., 2012). Despite the highly similar apparent localization in the subapical plasma membrane of the same cell (Figure 1B), strong transgenic expression of AtPIP5K2-EYFP or NtPIP5K6-EYFP resulted in distinct and divergent effects on cell morphology, as shown in Figure 1, C–G for AtPIP5K2, NtPIP5K2, NtPIP5K6, and for the chimeric enzyme variants 2swap6-EYFP and 6swap2-EYFP. Representative images of the respective pollen tube morphologies observed for each PI4P 5-kinase variant are shown in Figure 1C. While untransformed control pollen tubes or pollen tubes expressing an EYFP control displayed regular pollen tube growth, strong expression of AtPIP5K2-EYFP resulted in pronounced pollen tube tip swelling (Figure 1, C and D). Please note that catalytic activity was required for the tip swelling morphology, as the catalytically inactive variant AtPIP5K2 K470A did not cause pollen tube tip swelling when transgenically expressed (Figure 1, C and D). The strong expression of NtPIP5K2 resulted in pollen tube tip swelling indistinguishable from that caused by AtPIP5K2 (Figure 1, C and D). By contrast, strong expression of NtPIP5K6-EYFP resulted in pollen tube tip branching and in extensive apical pectin deposition, here stained by ruthenium red (Figure 1C). Please note that all pollen tubes shown in Figure 1C and analyzed for Figure 1E have been stained for equal periods with ruthenium red. The strong transgenic expression of the chimeric protein 2swap6-EYFP resulted in increased apical pectin deposition (Figure 1C), and that of the chimeric 6swap2-EYFP resulted in pollen tube tip swelling in addition to increased apical pectin deposition (Figure 1C), indicating shifted physiological effects of the chimeric proteins. Quantifications of the degrees of pollen tube tip swelling (Figure 1D) and of apical pectin deposition (Figure 1E) for all expressed constructs indicate a significant difference in the morphological effects resulting from the overexpressed PIP5K2 orthologs from Arabidopsis or tobacco, as compared to overexpressed NtPIP5K6. The data furthermore indicate that the chimeric enzyme variants, in which the Lin-domains were reciprocally swapped, displayed a largely reversed pattern of morphological effects, while retaining some of the original functionality of the respective parental enzymes. When the incidence of pollen tube cell morphologies was scored in transformed populations of pollen tubes upon the strong expression of the parental vs. the respective chimeric enzyme variants, expression of AtPIP5K2-EYFP resulted in pollen tube tip swelling and no detectable tip branching or stunted growth (Figure 1F). By contrast, strong expression of the chimeric 2swap6-EYFP resulted in the appearance of the stunted/branched morphology concomitant with a reduced incidence of swollen cells in the population of transgenic pollen tubes (Figure 1F). Reciprocally, strong expression of NtPIP5K6-EYFP resulted in an enhanced incidence of pollen tube tip branching and no detectable tip swelling, whereas the expression of the chimeric 6swap2-EYFP resulted in the appearance of the swollen tip morphology concomitant with a reduced incidence of branched cells (Figure 1G). Differences in phenotypic incidence were not due to different expression levels of the respective proteins, since fluorescence intensities of transformed pollen tubes displayed no significant differences (Figure 1, F and G, right panels).

Together, the side-by-side comparison of morphological effects of the transgenic expression of putative EYFP-tagged PIP5K2 orthologs from Arabidopsis or tobacco with those caused by expressed NtPIP5K6-EYFP in tobacco pollen tubes suggests that these enzymes may independently generate PtdIns(4,5)P_2 pools with respectively distinct regulatory effects on pollen tube growth. The determinants of such functional specification of PtdIns(4,5)P_2 effects are not understood. The comparison of AtPIP5K2/NtPIP5K2 and NtPIP5K6 effects on pollen tube morphologies provides the opportunity to elucidate the molecular mechanisms underlying alternative PtdIns(4,5)P_2 functions. The cell morphologies observed upon the strong transgenic expression of the chimeric enzyme variants 2swap6-EYFP and 6swap2-EYFP are consistent with a contribution of the Lin-domains in specifying the regulatory effects of PtdIns(4,5)P_2 produced by the respective PI4P 5-kinases tested.

PtdIns(4,5)P_2 forms membrane nanodomains in the subapical plasma membrane of tobacco pollen tubes

The presence of a plasma membrane region enriched in PtdIns(4,5)P_2 has previously been shown by confocal microscopy (Kost et al., 1999). To determine whether the postulated alternative effects of PtdIns(4,5)P_2 were accompanied by further spatial segregation of PtdIns(4,5)P_2 at a smaller

scale, we analyzed the distribution of RedStar-PLC-PH, a fluorescent biosensor for PtdIns(4,5)P_2, with high spatio-temporal resolution. In previous studies of membrane-associated protein complexes, the use of SD has enabled the observation of their lateral membrane distribution patterns at a scale resolving membrane nanodomains (Konopka et al., 2008; Sampathkumar et al., 2011; Gadeyne et al., 2014; Bloch et al., 2016; Synek et al., 2017). Therefore, we used SD to analyze the distribution of RedStar-PLC-PH in pollen tubes (Figure 2). In a median confocal section of a pollen tube transgenically expressing RedStar-PLC-PH, fluorescence was present only at the plasma membrane and possibly at the immediate periphery, but not in the volume of the cell, as indicated by confocal z-stacks of 0.3-µm slices projected in the xy, yz, and xz orientations (Figure 2A). A progression through the z-stack also illustrates that the volume of the pollen tube was devoid of RedStar-PLC-PH fluorescence (Figure 2B; Supplemental Movie 1), whereas a spotty fluorescence distribution was observed at the cell surface. A 3D-projection of the same image-stack clearly shows the presence of numerous punctate signals in addition to diffuse fluorescence in the plane of the membrane at the cell surface (Figure 2C; Supplemental Movie 2), indicating possible subcompartmentalization of PtdIns(4,5)P_2 in the plasma membrane of pollen tubes. Please note that the effect of the RedStar-PLC-PH biosensor on pollen tube growth rates was indistinguishable from that of an expressed EYFP control, and that the expression of either transgene had only a very mild effect compared to nontransformed pollen tubes (Supplemental Figure 2).

The plasma membrane nanodomains decorated by RedStar-PLC-PH (from now also referred to as "PtdIns(4,5)P_2 nanodomains") occurred in a region between 1 and 12 µm distant from the tips of both growing and nongrowing pollen tubes, with 50% of the nanodomains concentrating between 3 and 6 µm distance from the tip (Figure 2D). Within this region, the diameters of PtdIns(4,5)P_2 nanodomains did not substantially vary with increasing distance from the pollen tube tips and with no difference between growing or nongrowing tubes (Figure 2E). Detailed scrutiny of the RedStar-PLC-PH signal intensities quantified along the dashed lines in Figure 2, F and G indicated that the intensity of nanodomains decorated by the PtdIns(4,5)P_2 reporter was roughly two-fold higher than the diffuse reporter fluorescence in the membrane (Figure 2, F and G), which by itself was substantially above background (indicated by dashed lines in the intensity profiles in Figure 2, F and G). The SD analysis of pollen tubes expressing the RedStar-PLC-PH biosensor for PtdIns(4,5)P_2 thus indicates the presence of PtdIns(4,5)P_2 nanodomains in addition to diffuse reporter fluorescence within the subapical plasma membrane in a pattern consistent with spatially separated coexisting pools of PtdIns(4,5)P_2. The mean apparent diameters of the PtdIns(4,5)P_2 nanodomains were 0.7 ± 0.1 µm in growing and 0.6 ± 0.1 µm in nongrowing pollen tubes (Figure 2H), with the majority of nanodomains displaying diameters of approx. 0.6 µm in both growing and nongrowing pollen tubes (Figure 2I). To test for possibly unequal lipid distribution in the plasma membrane, tobacco pollen tubes were nonspecifically stained with the lipophilic membrane dye, Di-4 ANEPPDHQ (Figure 2J). During very weak labeling and with excitation at 488 nm, the fluorescence distribution of the dye displayed a spotty pattern (Figure 2J), suggesting an uneven distribution of lipids in the membrane.

PtdIns(4,5)P_2 nanodomains are highly dynamic

Punctate signals of the RedStar-PLC-PH biosensor at the cell surface were monitored over time in growing and nongrowing pollen tubes (Figure 3, A and B; Supplemental Movies 3–6). A kymograph analysis (Figure 3C) indicates dynamic behavior of the nanodomains with plasma membrane lifetimes between a few seconds and a few minutes (Figure 3D). In growing pollen tubes, approx. 75% of the PtdIns(4,5)P_2 nanodomains exhibited lifetimes of below 10 s (Figure 3D). While approx. 65% of PtdIns(4,5)P_2 nanodomains in nongrowing pollen tubes also had lifetimes below 10 s, the nongrowing cells additionally displayed a population of PtdIns(4,5)P_2 nanodomains with longer lifetimes of up to 2 min (Figure 3D). The incidence of PtdIns(4,5)P_2 nanodomain lifetimes above 60 s was found to be approx. four times higher in nongrowing than in growing cells (Figure 3D, inset). An analysis of the lifetimes of PtdIns(4,5)P_2 nanodomains at different distances from the pollen tube tip indicates that nanodomains with longer lifetimes occurred mostly further away from the tip in nongrowing pollen tubes, whereas the majority of the nanodomains with shorter lifetimes occurred significantly closer to the tip in growing pollen tubes (Figure 3E). The dynamic pattern of plasma membrane nanodomains decorated by the RedStar-PLC-PH biosensor is consistent with perpetual competitive recruitment of proteins to the nanodomains—possibly displacing the biosensor—and/or represents an active balance of PtdIns(4,5)P_2 biosynthesis and breakdown.

AtPIP5K2 occupies nanodomains whereas NtPIP5K6 displays uniform distribution in the plasma membrane of pollen tubes

To assess the biosynthesis of PtdIns(4,5)P_2 in this context, we monitored the lateral distribution of fluorescence-tagged variants of AtPIP5K2-EYFP, the catalytically inactive AtPIP5K2 K470A-EYFP, NtPIP5K2-EYFP, NtPIP5K6-EYFP or the chimeric variants 2swap6-EYFP and 6swap2-EYFP (see Figure 1A) in pollen tubes by SD (Figure 4). All constructs were transgenically expressed from the Lat52 promoter. Median confocal sections indicated association with the plasma membrane in all cases (Figure 4, A–F, top panels, as indicated). When confocal z-stacks of 0.3-µm slices were recorded and the frames representing the plasma membrane surface were visually examined, AtPIP5K2-EYFP, AtPIP5K2 K470A-EYFP, and NtPIP5K2-EYFP all associated with plasma membrane nanodomains (Figure 4, A–C, middle and

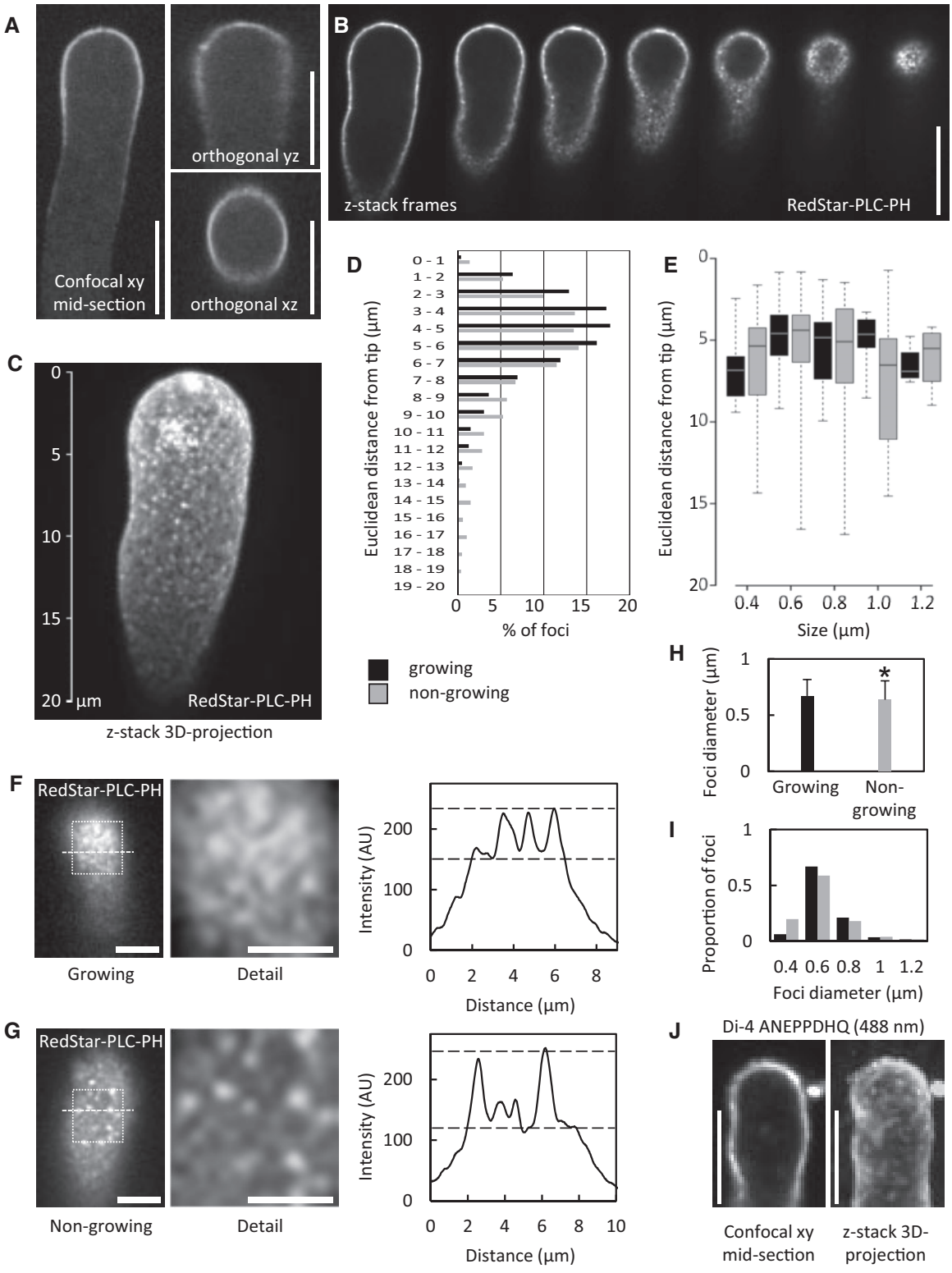

Figure 2 A PtdIns(4,5)P_2 biosensor decorates membrane nanodomains in the subapical plasma membrane of tobacco pollen tubes. The fluorescence distribution of the PtdIns(4,5)P_2-specific reporter RedStar-PLC-PH was monitored upon transient expression in tobacco pollen tubes by SD. A, Projections of confocal z-stacks with xy, yz, and xz orientations of a representative pollen tube expressing RedStar-PLC-PH. Scale bars, 10 µm. B, Sequence of images extracted from SD z-stack acquisition (0.3-µm slices) of tobacco pollen tubes expressing RedStar-PLC-PH (from median confocal plane to the cell surface). PtdIns(4,5)P_2 nanodomains are visible as bright dots at the cell surface. Please note the absence of fluorescence at the cell interior. Scale bar, 10 µm. C, 3D projection from a z-stack acquisition (0.3-µm slices) of a representative pollen tube expressing RedStar-PLC-PH. Scale as indicated. D, Distribution of PtdIns(4,5)P_2 nanodomains over the Euclidean distance from the pollen tube tip, as determined for growing pollen tubes (black bars) or for nongrowing pollen tubes (grey bars). The analysis is based on 8,881 nanodomains from 8 cells (growing)

bottom images, as indicated; Supplemental Movies 7–10), whereas NtPIP5K6-EYFP displayed a more uniform distribution (Figure 4D, middle and bottom images, as indicated). The substantial difference in the association of AtPIP5K2-EYFP/NtPIP5K2-EYFP with nanodomains vs. the more uniform lateral distribution of NtPIP5K6-EYFP was evident from the intensity plots (Figure 4, A–D, bottom panels) respectively recorded along the dashed lines in the detail views of the surface scans, as indicated. Interestingly, the nanodomain distribution of AtPIP5K2 K470A-EYFP indicates that catalytic activity as a PI4P 5-kinase is not required for nanodomain association (Figure 4B). When the plasma membrane distribution of AtPIP5K2-EYFP was additionally compared side-by-side to that of AtPIP5K5-EYFP, which causes apical pectin secretion and pollen tube branching upon overexpression in pollen tubes equivalent to NtPIP5K6 (Ischebeck et al., 2008, 2010b), again a difference in distribution patterns was observed by SD, with AtPIP5K2-EYFP in nanodomains and AtPIP5K5-EYFP displaying diffuse distribution similar to that observed for NtPIP5K6-EYFP (Supplemental Figure 3). The data indicate that the pollen tube tip swelling morphology is associated with AtPIP5K2-EYFP located in plasma membrane nanodomains, whereas "secretion phenotypes" are associated with NtPIP5K6-EYFP or AtPIP5K5-EYFP, which display a more continuous plasma membrane distribution.

To assess the role of the Lin-domains in mediating nanodomain vs. diffuse membrane patterns, we analyzed the distribution of the chimeric proteins 2swap6-EYFP and 6swap2-EYFP (Figure 4, E and F). In the 2swap6-EYFP chimera, the exchange of the Lin domain of AtPIP5K2 for that of NtPIP5K6 did not fully abolish nanodomain association of the 2swap6-EYFP fusion when compared to the parental AtPIP5K2-EYFP protein (Figure 4E). This distribution pattern, as indicated by the surface scan and the corresponding line intensity plot (Figure 4E) suggests that besides the Lin domain additional features of the AtPIP5K2 protein may favor nanodomain association. The reciprocal 6swap2-EYFP chimera displayed substantially enhanced association with membrane nanodomains when compared to the uniform distribution of the parental NtPIP5K6-EYFP protein, as indicated by the surface scan and line intensity plot (Figure 4F), indicating that the Lin-domain of AtPIP5K2 can confer a significant degree of nanodomain association to the NtPIP5K6-EYFP protein.

As the comparison of line intensity patterns might be subject to experimental bias (e.g. through the manual positioning of the dashed line), we applied a nonbiased analysis based on the standard deviations of pixel intensity values from multiple images recorded by SD at the cell surface. High standard deviations among intensity values reflect a heterogeneous distribution of fluorescence intensity values, and therefore indicate the presence of nanodomains at the membrane. By contrast, low standard deviations reflect a more homogeneous distribution of intensity values and therefore a diffuse distribution of the fluorescence at the membrane. The standard deviations for surface scans of pollen tubes transgenically expressing AtPIP5K2-EYFP, NtPIP5K6-EYFP, 2swap6-EYFP, or 6swap2-EYFP are given in Figure 4G and correspond well with the data from the visual examination and from the line intensity plots (Figure 4, A–F).

The plasma membrane nanodomains decorated by AtPIP5K2-EYFP were dynamic (Supplemental Movies 7–10) and the analysis of their lifetime distribution (Figure 4H) resembled that of RedStar-PLC-PH nanodomains (see Figure 2D), with more than 60% of nanodomains having lifetimes shorter than 10 s. Interestingly, we observed a small percentage (approx. 5%) of AtPIP5K2-EYFP nanodomains with longer lifetimes (>2 min) in a similar pattern as with RedStar-PLC-PH nanodomains from nongrowing pollen tubes (see Figure 2D).

Overall, the different lateral plasma membrane distributions of AtPIP5K2-EYFP and NtPIP5K6-EYFP appear to correlate with the divergent respective functionalities of the enzymes. The divergent membrane distribution patterns support the notion that subcompartmentalization of PtdIns(4,5)P_2 production by these enzymes may underlie the functional specification of PtdIns(4,5)P_2 regulatory effects. The data furthermore support a role for the Lin-domain as

Figure 2 (Continued)
or 17,204 nanomonains from 10 cells (nongrowing). E, Size distribution of nanodomains decorated by RedStar-PLC-PH along the tips of growing (black bars) or nongrowing pollen tubes (grey bars) over the Euclidean distance from the pollen tube tip. Data represent 221 nanodomains from 8 cells (growing); or 227 nanodomains from 10 cells (nongrowing), respectively. For the box plots, quartiles were first defined by numerically ordering the recorded values: The median divides the number of values in two halves, which are each further divided into quartiles. The ends of the box represent the upper and lower quartiles of recorded values, so the box spans the interquartile range. The median of all recorded values is marked by a horizontal line inside the box. The whiskers extend to the highest and lowest recorded values. F, G, The intensities of PtdIns(4,5)P_2 nanodomains decorated by RedStar-PLC-PH were recorded by SD in cell surface scans of growing (F) or nongrowing pollen tubes (G). Left panels, representative SD images of the cell surface. Scale bars, 5 μm. White boxes, regions of interest enlarged in middle panels (scale bars there, 3 μm). Right panels, fluorescence intensity plots derived from dashed lines in left panels. Dashed lines in the intensity plots, estimated levels of diffuse marker fluorescence (lower line) and of nanodomain fluorescence (upper line). H, Mean nanodomain diameters were calculated for growing (black bar) or nongrowing pollen tubes (grey bar) from the data shown in (E). Data are given as means ± standard deviation. The asterisk indicates a significant difference according to a Student's *t* test (*$p \leq 0.05$). I, The distribution of size categories of nanodomain diameters was scored in growing (black) and in nongrowing pollen tubes (grey). The distribution was calculated from the same data as shown in (H). J, Tobacco pollen tubes were stained with the membrane dye, Di-4 ANEPPDHQ, to test for unequal lipid distribution in the plasma membrane. During very weak labeling and with excitation at 488 nm, a spotty fluorescence distribution was observed. The cell shown is a growing pollen tube and representative for 12 stained cells observed.

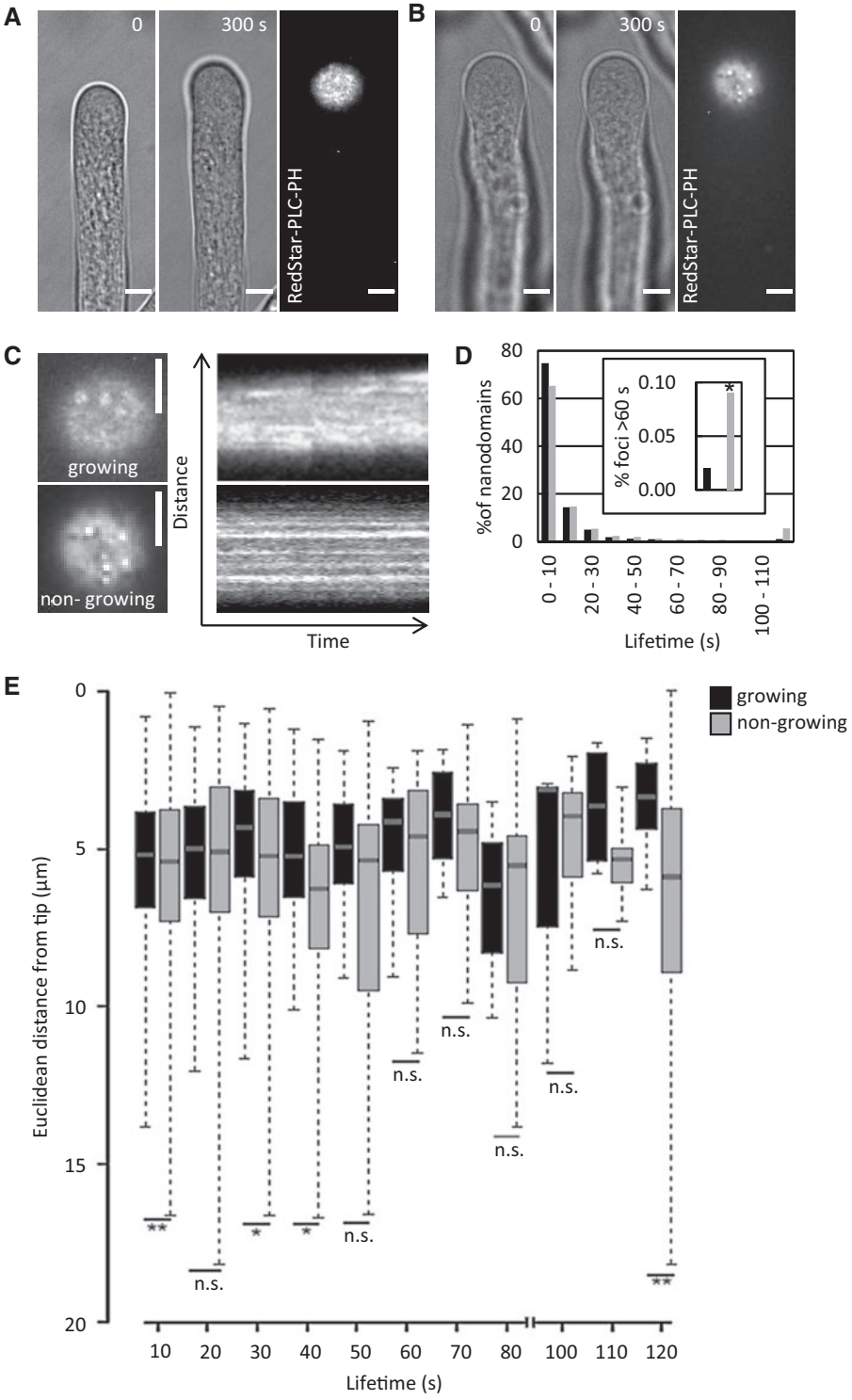

Figure 3 RedStar-PLC-PH-labeled PtdIns(4,5)P_2 nanodomains are dynamic. The dynamics of PtdIns(4,5)P_2 nanodomains at the cell surface were recorded by SD in tobacco pollen tubes upon the transient expression of the RedStar-PLC-PH biosensor from the Lat52 promoter. A, B, PtdIns(4,5)P_2 nanodomains in a growing (A) or nongrowing tobacco pollen tube (B). Left panels, growth or no growth of the pollen tube according to bright field image frames from image acquisition over a period of 5 min at 0.5 frames s^{-1}; only the first and last frames are shown. Right panels, SD imaging of the last frames from the same pollen tubes with the confocal plane focused at the PtdIns(4,5)P_2 nanodomains at the cell surface. Scale bars, 5 µm. C, Kymograph analysis of the image sequences obtained for growing (upper panels) or nongrowing cells (lower panels). Left, fluorescence images at the cell surface (magnified from images in (A) and (B). Scale bars, 5 µm. Right panels, Kymographs from the same pollen tubes over a period of 5 min. D, Life time distribution of dynamic PtdIns(4,5)P_2 nanodomains decorated by RedStar-PLC-PH in growing (black bars) or nongrowing pollen tubes (grey bars). Data represent 1,415 tracks from eight cells (growing) or 3,203 tracks from 16 cells (nongrowing pollen tubes). Inset, total percentage of nanodomains with lifetimes between 60 and 120 s in growing (black bar) or nongrowing pollen tubes

one factor contributing to nanodomain association or uniform membrane association of PI4P 5-kinases, thereby directing PI4P 5-kinases into different regulatory contexts.

AtPIP5K2-EYFP and PtdIns(4,5)P_2 nanodomains occur in a spatially correlated pattern at the plasma membrane

The results so far indicated the presence of plasma membrane nanodomains with similar dynamics for PtdIns(4,5)P_2 and AtPIP5K2-EYFP. Therefore, we next characterized the spatial distribution of nanodomains occupied by AtPIP5K2-EYFP at the plasma membrane in more detail. Confocal z-stacks of 0.3-µm slices acquired by SD indicate that AtPIP5K2-EYFP fluorescence was limited to the cell surface, with little or no fluorescence in the volume of the cell (Figure 5A, image series in left panel). A 3D-projection of the z-stack shows the presence of punctate signals at the cell surface (Figure 5A, right panel). Membrane association of the AtPIP5K2-EYFP marker was assessed by costaining with the lipophilic dye, FM 4-64 (Figure 5, B and C). While the distribution of AtPIP5K2-EYFP coincided with that of FM 4-64 (Figure 5C), we noted a small but reproducible right shift of the AtPIP5K2-EYFP signal (Figure 5C), suggesting that AtPIP5K2-EYFP occupied a peripheral region further inside the cell than the plasma membrane dye. This result is supported by the patterns observed upon the coexpression of AtPIP5K2-EYFP together with the PtdIns(4,5)P_2 biosensor RedStar-PLC-PH, where we also observed a small spatial distinction with the AtPIP5K2-EYFP marker localizing further inward from the plasma membrane into the cell periphery (Figure 5D). To verify the optical alignment of the two fluorescence channels of our microscopic setup, a control experiment was performed by costaining pollen tubes with a red (FM 4-64) and a green dye (FM 1-43) and analyzing the relative fluorescence distributions. In this analysis no positional shift between the red and green fluorescence channels was observed (Supplemental Figure 4).

Both the PtdIns(4,5)P_2-biosensor and the AtPIP5K2-EYFP marker displayed membrane nanodomain association at the cell surface when analyzed by SD, so we next asked whether the distribution patterns of these markers were spatially correlated. To assess the relative distribution patterns of AtPIP5K2-EYFP and RedStar-PLC-PH, we attempted to analyze flattened images from 3D-projections of cells coexpressing both markers, such as shown in Figure 5D. Due to the density of the signals, however, colocalizing signals in these analyses could not be distinguished from random coincidence. To nonetheless provide a measure of the relative positioning of AtPIP5K2-EYFP and RedStar-PLC-PH distributions, we resorted to the quantitative analysis of median confocal sections (Figure 5, E and F), which display lesser complexity. Interestingly, inspection of median confocal sections of pollen tubes revealed that high fluorescence intensity values from AtPIP5K2-EYFP and RedStar-PLC-PH displayed similar localizations at the plasma membrane (Figure 5E). Fluorescence signals from multiple stacks were therefore analyzed by summing the intensity values of the vertical pixel columns for each fluorescence channel (AtPIP5K2-EYFP and RedStar-PLC-PH in Figure 5E; for details, please see the Materials and methods section and Supplemental Figure 5). Detail patterns for the individual fluorescence channels are given for a representative pollen tube in Figure 5F. The resulting sum intensity profiles (Figure 5G) provide a measure for the intensity distribution along the curved plasma membrane surface of the pollen tube cells. The sum intensity profiles thus obtained for AtPIP5K2-EYFP and for RedStar-PLC-PH display similar detail patterns (Figure 5G). Correlation analysis of the fluorescence patterns, which can be numerically assessed by calculating the corresponding Pearson coefficient R, which can range from 0 (no correlation) to 1 (perfect correlation), was performed and is shown for one representative pollen tube in Figure 5H (upper panel; $R = 0.933$). The analysis of pollen tube cells coexpressing both markers (16 cells, each with five individual measurements) consistently indicates a tight correlation of the markers with a mean R-value of 0.90 (Figure 5H, lower panel).

Together, the data indicate that AtPIP5K2-EYFP distributes in the plasma membrane in a nanodomain pattern that is spatially correlated to the positioning of the PtdIns(4,5)P_2-biosensor and additionally reaches inward towards the cytoplasmic periphery.

AtPIP5K2-EYFP controls the dynamic actin cytoskeleton in pollen tubes

As pollen tube tip swelling morphology, such as that observed upon the strong transgenic expression of AtPIP5K2-EYFP or NtPIP5K2-EYFP (Figure 1, C–G), has previously been linked to changes in the actin cytoskeleton (Klahre et al., 2006; Klahre and Kost, 2006; Kost, 2008; Ischebeck et al., 2011), we further investigated the effects of different PI4P 5-kinases on pollen tube actin (Figures 6–7). To assess regulation of the pollen tube actin cytoskeleton by AtPIP5K2-EYFP, we monitored actin in pollen tubes coexpressing variants of AtPIP5K2 or NtPIP5K6 together with the in vivo actin markers LifeAct-mCherry (Riedl et al., 2008; Vidali et al., 2009; Lichius and Read, 2010) or mTalin-YFP (Kost et al., 1998; Fu et al., 2001; Figures 6–7). The

Figure 3 (Continued)
(grey bar). E, Distribution of lifetimes of PtdIns(4,5)P_2 nanodomains over the Euclidean distance from the tips of growing (black bars) or nongrowing pollen tubes (grey bars). For the box plots, quartiles were first defined by numerically ordering the recorded values: the median divides the number of values in two halves, which are each further divided into quartiles. The ends of the box represent the upper and lower quartiles of recorded values, so the box spans the interquartile range. The median of all recorded values is marked by a horizontal line inside the box. The whiskers extend to the highest and lowest recorded values. Asterisks indicate significant differences between the corresponding values (lifetimes or distances) according to a Student's t test (**$P \leq 0.01$; *$P \leq 0.05$; n.s., not significant).

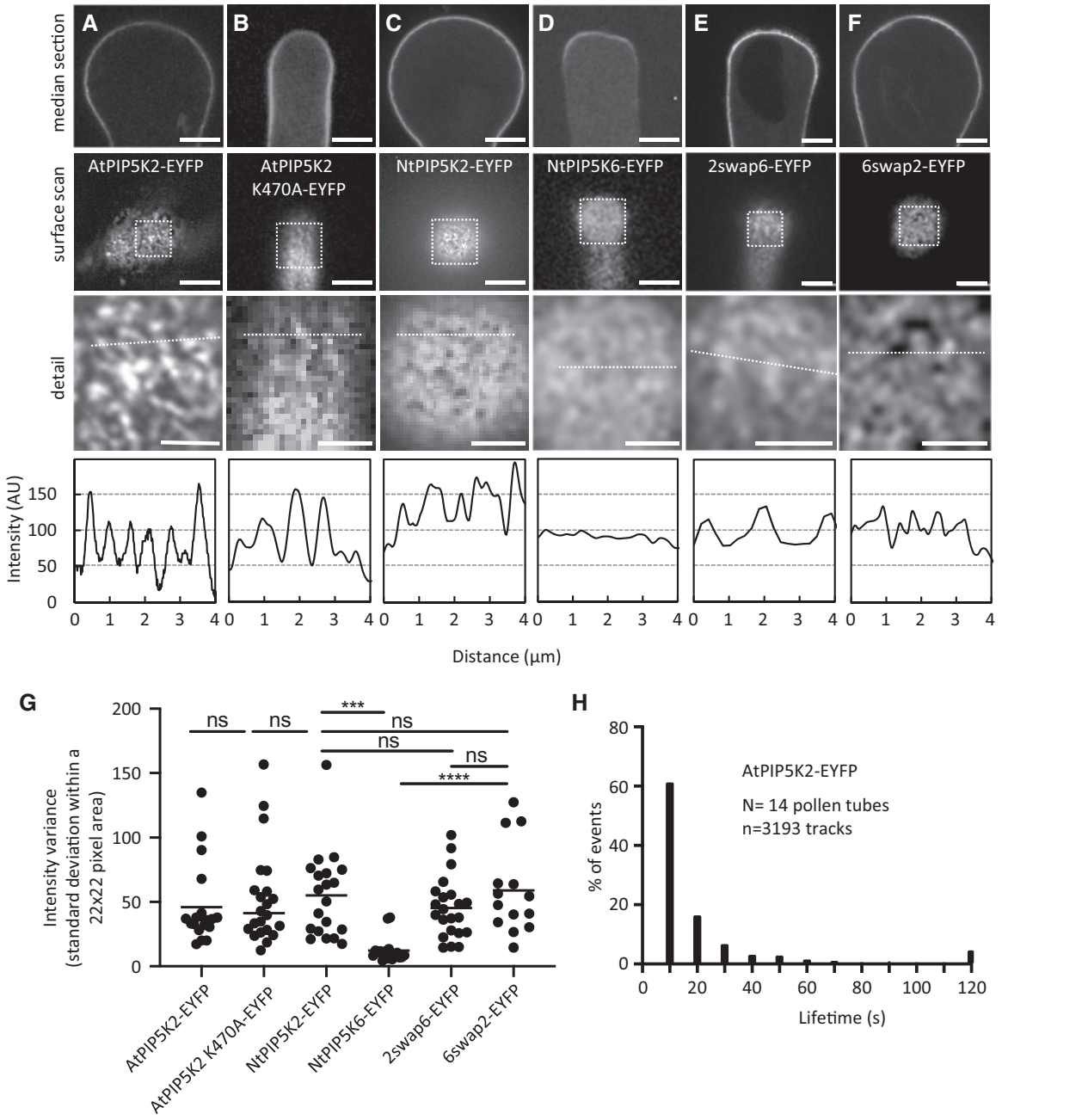

Figure 4 AtPIP5K2-EYFP occupies nanodomains whereas NtPIP5K6-EYFP displays uniform distribution in the plasma membrane. The fluorescence distribution of AtPIP5K2-YFP, the catalytically inactive AtPIP5K2 K470A-EYFP, NtPIP5K2, NtPIP5K6-YFP, or the chimeric variants 2swap6-EYFP or 6swap2-EYFP at the plasma membrane was monitored by SD upon transient expression in tobacco pollen tubes from the Lat52 promoter. A, AtPIP5K2-EYFP; B, AtPIP5K2 K470A-EYFP; C, NtPIP5K2-EYFP; D, NtPIP5K6-EYFP; E, 2swap6-EYFP; F, 6swap2-EYFP. Top images, Median confocal sections of representative pollen tubes showing the fluorescence signal at the plasma membrane. Center images, surface scan of the same cells extracted from z-stack acquisition (0.3-µm slices). White boxes, areas of interest enlarged in bottom images, giving a detail view of the distribution of the fusion proteins at the plasma membrane, as indicated. Bottom panels, fluorescence intensity plots derived from the dashed lines in the magnified detail images. Scale bars, 5 µm. G, Nonbiased assessment of uniformity of fluorescence intensity distributions according to the standard deviations of the overall fluorescence intensity values. The standard deviations of all intensity values in a 22 × 22 pixel area of an image were calculated as a measure of uniformity for cells expressing AtPIP5K2-EYFP ($N = 19$); AtPIP5K2 K470A-EYFP ($N = 22$); NtPIP5K2-EYFP ($N = 20$); NtPIP5K6-EYFP ($N = 17$); 2swap6-EYFP ($N = 22$); and 6swap2-EYFP ($N = 14$). Asterisks indicate significant differences according to a Student's *t* test (****$P \leq 0.0001$; ***$P \leq 0.001$; n.s., not significant). H, Lifetime distribution of AtPIP5K2-EYFP nanodomains. Pollen tubes expressing AtPIP5K2-YFP were imaged by SD at a frame rate of 0.5 frames s^{-1} for 2 min. The distribution of lifetimes is given based on 3,193 tracks recorded from 14 cells.

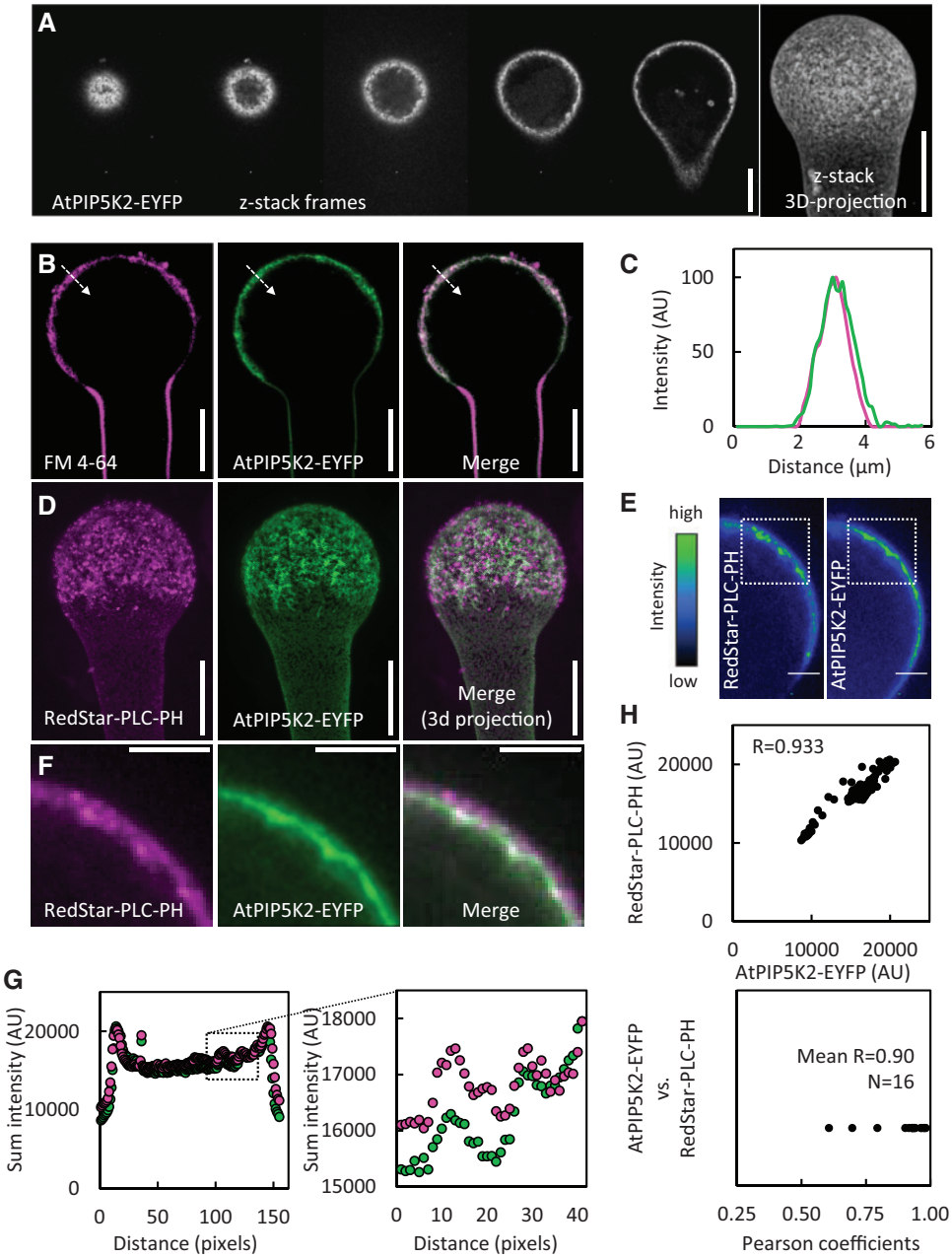

Figure 5 AtPIP5K2-EYFP and PtdIns(4,5)P_2 nanodomains occur in a spatially correlated pattern at the plasma membrane. The fluorescence distribution of AtPIP5K2-YFP and RedStar-PLC-PH at the plasma membrane was observed by SD or LSM upon transient expression in tobacco pollen tubes from the Lat52 promoter. A, Representative sequence of images extracted from SD z-stack acquisition (0.3-μm slices) of a tobacco pollen tube expressing AtPIP5K2-EYFP (left to right, from cell surface to median confocal section). Right image, 3D projection obtained from the same full z-stack acquisition. AtPIP5K2-EYFP nanodomains are visible as bright dots at the cell surface. Scale bars, 10 μm. B, Representative LSM images of a tobacco pollen tube expressing AtPIP5K2-YFP and costained with the membrane dye, FM 4-64, as indicated. Scale bars, 10 μm. C, Fluorescence intensity plot derived from the dashed line across the plasma membrane, as indicated in (B). D, A representative 3D reconstruction from SD z-stack acquisition (0.3-μm slices) of a pollen tube coexpressing the PtdIns(4,5)P_2 biosensor RedStar-PLC-PH and AtPIP5K2-EYFP, as indicated. Right panel, merged image. Scale bar, 10 μm. E, Representative median confocal frames extracted from the z-stack projection shown in (D) and representing the individual channels for RedStar-PLC-PH and AtPIP5K2-EYFP with heatmap colors, as indicated. Note that high intensity values from both channels localize in the same areas at the cell periphery. Scale bars, 2 μm. F, Detail fluorescence micrographs of the regions of interest indicated by the white boxes in (E), as indicated. Scale bars, 2 μm. G, The sum intensities were determined for the vertical pixel columns of each channel (please refer to Supplementary Figure 5 and Materials and methods section for details). Left panel, Sum intensities for RedStar-PLC-PH (red) and AtPIP5K2-EYFP (green); right panel, detailed view if the region of interest indicated by the box in the left panel. H, Correlation analysis of sum intensity profiles obtained for RedStar-PLC-PH and AtPIP5K2-EYFP. Upper panel, representative correlation plot for the fluorescence distributions given in (G). The correlation is characterized by a high Pearson coefficient R of 0.933. Lower panel, Pearson coefficients obtained accordingly from 16 correlation analyses, with a mean R of 0.9, indicating consistently high correlations between the spatial distributions of RedStar-PLC-PH and AtPIP5K2-EYFP.

distribution of actin in the pollen tube tip of cells coexpressing PI4P 5-kinase variants with LifeAct-mCherry was visually examined in confocal z-stacks of 0.3-µm slices obtained by SD (Figure 6A, as indicated) and was quantitatively assessed according to the occupancy of the actin signal in the apical region of the cells (Figure 6B). Pollen tubes coexpressing LifeAct-RFP with an EYFP control did not have detectable actin structures in the apical region of the cells (Figure 6A, as indicated). By contrast, cells strongly expressing AtPIP5K2-EYFP and displaying tip swelling were characterized by an increased abundance of actin filaments in the apical region (Figure 6A, as indicated). Differences were highly significant according to the actin occupancy measurements (Figure 6B). Pollen tubes overexpressing NtPIP5K6-EYFP or the 2swap6-EYFP chimera displayed no or only weak tip swelling, respectively (Figure 6A, as indicated) and displayed significantly less actin occupancy in the tip compared to AtPIP5K2-EYFP (Figure 6B). Tip swelling was observed upon the strong transgenic expression of the 6swap2-EYFP chimera (Figure 6A, as indicated) and was accompanied by a significantly increased apical actin occupancy compared to the pattern observed with the parental NtPIP5K6-EYFP (Figure 6B). In these experiments, the membrane association of the PI4P 5-kinase variants did not differ, as determined by the ratios of plasma membrane/cytosolic fluorescence intensities in median confocal planes observed for the different markers, as indicated (Figure 6C).

The data indicate a significantly increased actin occupancy in the pollen tube tip of cells displaying tip swelling upon the strong expression of AtPIP5K2-EYFP. The data obtained with 2swap6-EAFP and 6swap2-EYFP indicate the manifestation of intermediate actin distributions when compared to the effects of the parental enzymes, AtPIP5K2 and NtPIP5K6, and correspond well with the intermediate morphological phenotypes observed upon the expression of these chimeric variants (see Figure 1). This observation suggests that, despite their significant effects, the Lin-domains swapped in the chimeras are likely not the only determinants of functional specification of the PI4P 5-kinases tested.

Next, the dynamic motility of actin filaments was assessed by observing growing and nongrowing pollen tubes coexpressing different PI4P 5-kinase variants with the live actin marker mTalin-YFP (Figure 7; Supplemental Movies 11–18). Actin dynamics were recorded over a period of 5 min by time-resolved laser scanning microscopy (LSM) imaging of z-stacks of 2-µm slices and subsequent kymographic analysis of maximum intensity projections (Figure 7A). The motility of actin traces was then quantified according to the kymographs (Figure 7, B and C). Growing and nongrowing pollen tubes coexpressing mTalin-YFP with an mCherry control displayed highly motile actin filaments that were mostly excluded from the pollen tube tip (Figure 7A, as indicated). By contrast, actin fibers decorated by mTalin-YFP in cells strongly expressing AtPIP5K2-mCherry or NtPIP5K2-mCherry were substantially stabilized, as evident from the thickness of the observed filaments as well as from the presence of horizontal lines in the kymographic analysis (Figure 7A, as

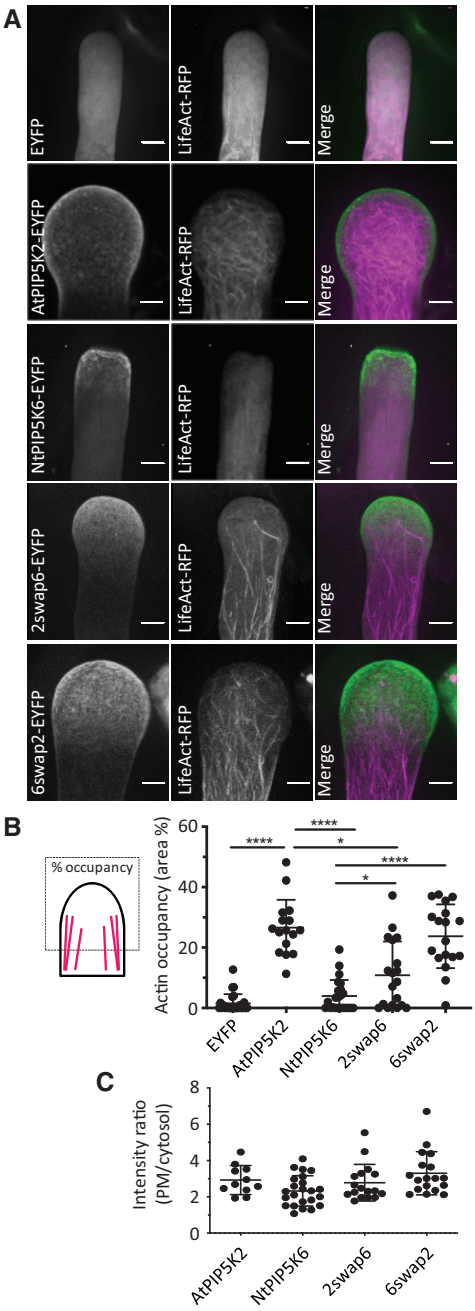

Figure 6 AtPIP5K2-EYFP influences actin distribution in pollen tubes. The actin cytoskeleton was monitored in vivo by SD in tobacco pollen tubes upon the coexpression of LifeAct-RFP respectively with an EYFP control, AtPIP5K2-EYFP, AtPIP5K2 K470A-mcherry, NtPIP5K2-mcherry, NtPIP5K6-EYFP, 2swap6-EYFP, or 6swap2-EYFP, as indicated. A, Representative 3D projections from z-stack acquisition (0.3-µm slices) are shown for the individual fluorescence channels and the merge, as indicated. Scale bars, 5 µm. B, Occupancy of the LifeAct-RFP signal in the pollen tube tips. Data are from 26 cells (LifeAct-RFP/EYFP); 16 cells (LifeAct-RFP/AtPIP5K2-EYFP); 23 cells (LifeAct-RFP/NtPIP5K6-EYFP) 18 cells (LifeAct-RFP/2swap6-EYFP); or 19 cells (LifeAct-RFP/6swap2-EYFP), respectively. Asterisks indicate significant differences according to a Student's *t* test, as indicated (****$P \leqslant 0.0001$; *$P \leqslant 0.05$). C, Membrane association of the PI4P 5-kinase variants was assessed by calculating the ratio of plasma membrane (PM)-associated fluorescence and cytosolic fluorescence from the images used for the analysis in (B), with no statistical differences between the distributions.

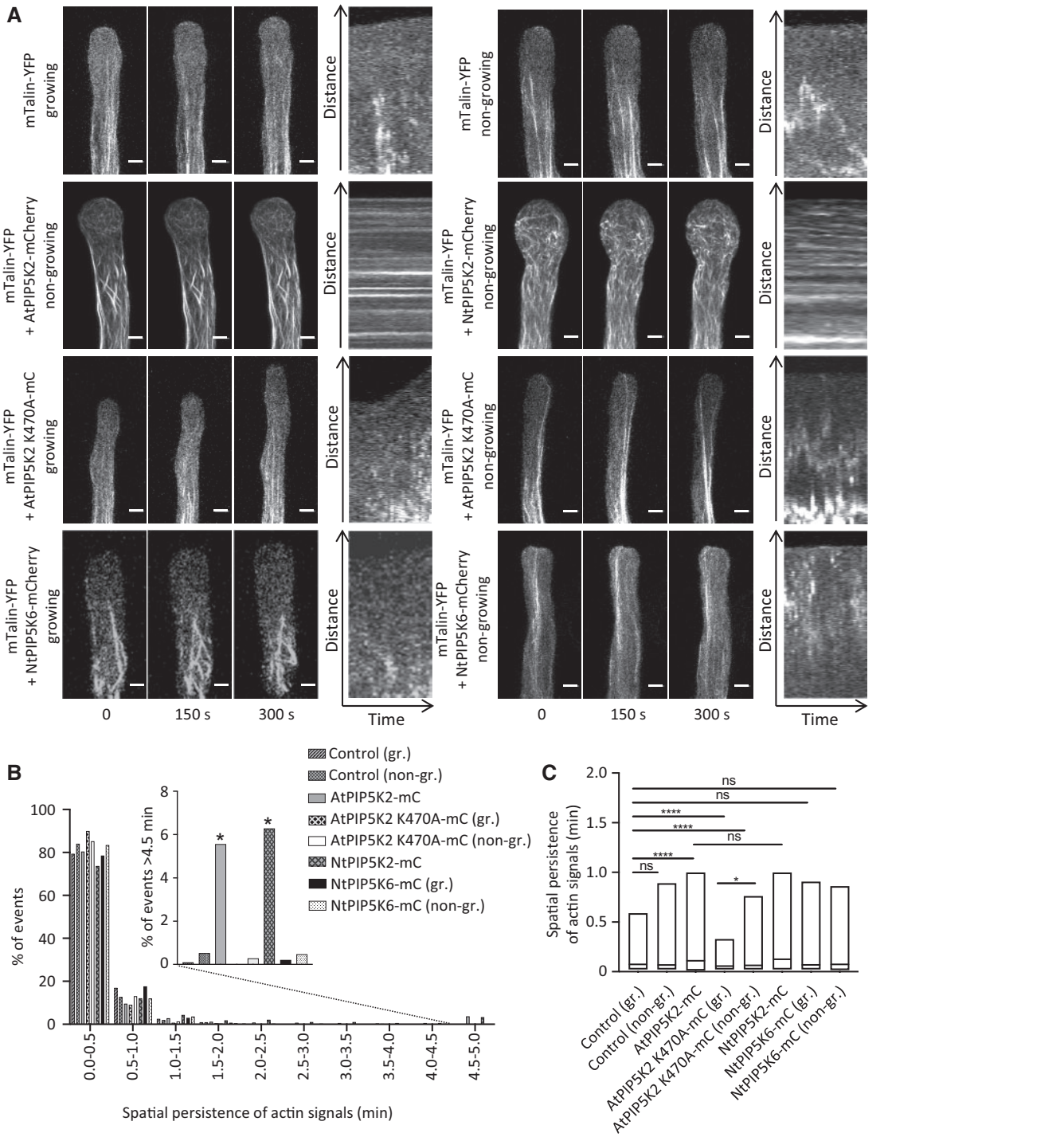

Figure 7 PIP5K2 orthologs influence actin dynamics in pollen tubes. Actin cytoskeletal dynamics were monitored in vivo by LSM in tobacco pollen tubes upon the coexpression of LifeAct-RFP respectively with controls or PI4P 5-kinase variants. A, The dynamics of the actin cytoskeleton was monitored in tobacco pollen tubes coexpressing the in vivo actin marker mTalin-YFP with either an mCherry control, or with AtPIP5K2-Cherry, NtPIP5K2-Cherry, AtPIP5K2 K470A-Cherry or NtPIP5K6-Cherry, as indicated. Time series of z-stacks were acquired by LSM for 2-µm slices at 0.1 frames s^{-1} over a period of 5 min. Images in the left panels show representative maximum intensity projections of the mTalin-YFP channel of pollen tubes observed at t = 0, t = 150 s, and t = 300 s for growing or nongrowing pollen tubes, as indicated. Right panels, representative kymograph analyses of the mTalin-YFP channel. Please note that horizontal lines indicate structures labeled by mTalin-YFP that remained static over the recorded period. Scale bars, 5 µm. B, The spatial persistence of the mTalin-YFP fluorescence was extracted from kymographs and plotted (for details of this analysis, please also see the Materials and methods section). Data represent 12 cells (mTalin-YFP/mCherry, growing); 10 cells (mTalin-YFP/mcherry, nongrowing); 21 cells (mTalin-YFP/AtPIP5K2-mcherry); 8 cells (mTalin-YFP/AtPIP5K2 K470A-mcherry growing pollen tubes); 11 cells (mTalin-YFP/AtPIP5K2 K470A-mcherry nongrowing pollen tubes); 7 cells (mTalin-YFP/NtPIP5K2-mcherry); 7 cells (mTalin-YFP/NtPIP5K6-mCherry growing pollen tubes); and 15 cells (mTalin-YFP/NtPIP5K6-mCherry, nongrowing). Inset, the percentage of mTalin-YFP kymograph signals persisting for a period of >4.5 min was plotted, and a significantly higher incidence of persisting signals was found upon the

indicated). Please note that despite the substantial stabilization of actin upon the strong expression of AtPIP5K2-mCherry, there was still an abundance of highly motile actin filaments recorded (Figure 7B), indicating that the actin cytoskeleton was still largely functional. It is possible that these fast signals in part reflect fluorescence background noise, which cannot easily be distinguished from true actin signals, and may thus be overrepresented in our analysis. Nonetheless, significantly reduced motility of actin filaments was observed in a minor (and thus possibly underestimated) proportion of filaments in cells strongly expressing AtPIP5K2-mCherry or NtPIP5K2-mCherry (Figure 7B, inset). Please also note that the expression of AtPIP5K2-EYFP at a level required to analyze effects associated with tip swelling precluded the observation of growing pollen tubes. The stabilizing effect of AtPIP5K2-mCherry on actin dynamics required catalytic activity of the enzyme, as strong expression of the catalytically inactive AtPIP5K2 K470A-mCherry variant did not result in reduced actin dynamics in growing or in nongrowing pollen tubes (Figure 7, A–C, as indicated). Instead, the quantitative analysis suggests an even faster average actin motility upon the expression of AtPIP5K2 K470A-mCherry, possibly in consequence of a dominant negative effect (Figure 7, B and C). When NtPIP5K6-mCherry and mTalin-YFP were coexpressed in pollen tubes, the actin marker displayed highly motile actin filaments, as evident from the kymographs by the absence of horizontal lines (Figure 7A, as indicated) and from the quantitative measurements (Figure 7, B and C, as indicated).

The quantitative analysis of actin motility shows that enhanced PtdIns(4,5)P_2 formation upon the strong transgenic expression of AtPIP5K2-mCherry or NtPIP5K2-mCherry resulted in a significant stabilization of prominent apical actin filaments, concomitant with substantial remaining motility of actin filaments of smaller scale.

Coordinated localization, interaction, and functional interplay of AtPIP5K2 with the actin regulator NtRac5

Based on the effects of AtPIP5K2 on actin dynamics, we next aimed to elucidate the molecular basis of PtdIns(4,5)P_2-dependent regulation of the actin cytoskeleton. Among the known regulators of plant actin dynamics, monomeric GTPases of the ROP family are among the best characterized (Kost et al., 1998; Fu et al., 2001; Yalovsky et al., 2008; Poraty-Gavra et al., 2013; Bloch et al., 2016). For the tobacco ROP NtRac5 a link to PtdIns(4,5)P_2-dependent pollen tube tip swelling has previously been suggested (Kost, 2008; Ischebeck et al., 2011). Importantly, localization of the closely related Arabidopsis ROP6 in plasma membrane nanodomains has recently been demonstrated. Therefore, we next addressed the effects of AtPIP5K2-EYFP on ROP signaling (Figure 8). First, the plasma membrane distribution of AtPIP5K2-EYFP and a coexpressed NtRac5-RFP marker was analyzed by SD (Figure 8, A–E). The maximum intensity projection of confocal z-stacks (0.3-µm slices) indicated a general enhanced apical localization of both markers in the pollen tube tip (Figure 8A), consistent with distribution patterns previously reported for either marker alone (Klahre et al., 2006; Klahre and Kost, 2006; Yalovsky et al., 2008; Stenzel et al., 2012; Grebnev et al., 2017). At a smaller scale, the detailed analysis of the distribution at the membrane surface indicated membrane nanodomains for both AtPIP5K2-EYFP and NtRac5-RFP (Figure 8B). Plasma membrane nanodomains appeared to cluster into larger islands colabeled by both markers (Figure 8, A and B). The density of the nanodomain signals at the plasma membrane precluded meaningful evaluation of colocalization patterns, which might arise as a consequence of random spatial coincidence. Therefore, we resorted to the quantitative analysis of multiple imaging stacks of lesser complexity as shown in Figure 8C, where high intensity signals displayed similar localization between AtPIP5K2-EYFP and NtRac5-RFP (boxes in Figure 8C). Fluorescence signals of multiple z-stacks around the median confocal section were analyzed for the sum intensity of the vertical pixel columns (for details, please see the Materials and methods section and Supplemental Figure 5). The resulting sum intensity profiles for AtPIP5K2-EYFP and for NtRac5-RFP displayed similar patterns, shown for a representative pollen tube in Figure 8, C and D (Figure 8D upper panel, full range; lower panel, detail), and a tight correlation of fluorescence intensity patterns with a high Pearson coefficient of $R = 0.95$ (Figure 8E, left panel). The analysis of pollen tube cells coexpressing both markers ($N = 11$ cells, each with five individual measurements) indicates a close correlation of the markers with a mean R-value of 0.87 (Figure 8E, right panel).

As AtPIP5K2-EYFP and NtRac5-RFP displayed spatially correlated distribution patterns, we next tested for interaction between the AtPIP5K2 and NtRac5 proteins (Figure 8, F and G). An interaction of AtPIP5K2 and NtRac5 in a protein complex is supported by split-ubiquitin-based yeast-two-hybrid analysis, in which cell growth on the restrictive −LTH media indicates positive interaction (Figure 8F), as assessed

Figure 7 (Continued)
coexpression of the mTalin-YFP marker with AtPIP5K2-mCherry or with NtPIP5K2-mCherry, indicating a stabilizing effect of both PIP5K2 orthologs, but none of the other fusions tested, on actin dynamics. The asterisks indicate a significant difference from the control (mTalin-YFP/mCherry, nongrowing) according to a Student's t test (*$P \leq 0.05$). C, The data on spatial persistence were plotted for each expressed construct to illustrate the mean respective effects on dynamic actin motility, as indicated. For the box plots, quartiles were first defined by numerically ordering the recorded values: The median divides the number of values in two halves, which are each further divided into quartiles. The ends of the box represent the upper and lower quartiles of recorded values, so the box spans the interquartile range. The mean of the recorded values is marked by a horizontal line inside the box. The whiskers extend to the highest and lowest recorded values. The asterisks indicate significant differences between constructs as indicated according to Student's t test (****$P \leq 0.0001$; *$P \leq 0.05$; n.s., not significant).

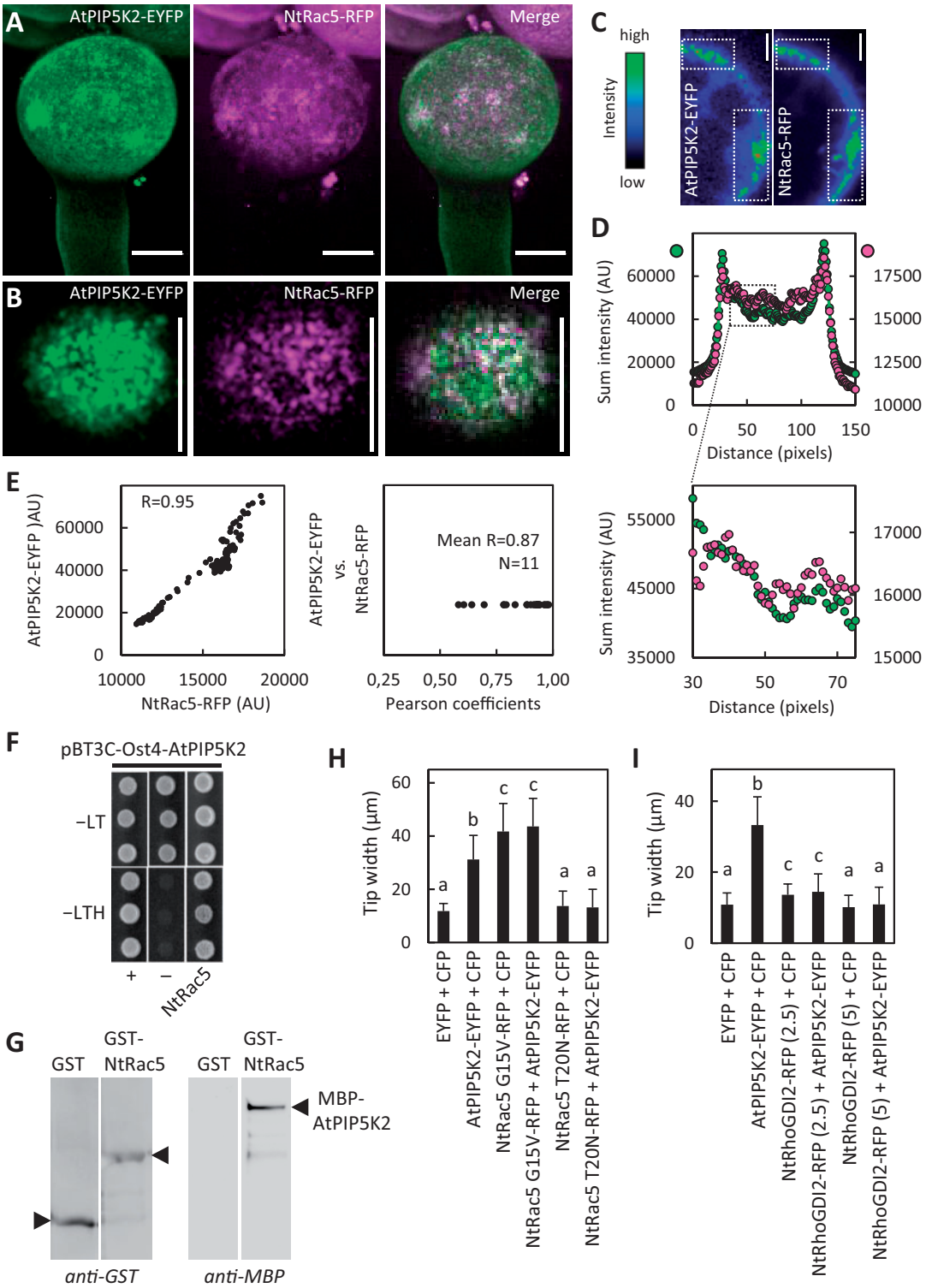

Figure 8 Coordinated localization, interaction and functional interplay of AtPIP5K2 with the actin regulator NtRac5. To explore the molecular mechanism by which AtPIP5K2 might influence actin dynamics, we tested for links to elements of ROP signaling, which are known to influence pollen tube actin. AtPIP5K2-EYFP was coexpressed with the tobacco ROP, NtRAC5-RFP, and fluorescence distributions were monitored by SD. A, Representative 3D reconstruction from z-stack acquisition (0.3-µm slices) of a pollen tube coexpressing AtPIP5K2-YFP and NtRAC5-RFP, as indicated. Scale bars, 10 µm. B, Fluorescence distribution at the cell surface of the pollen tube shown in (A), as indicated. Note that plasma membrane nanodomains of both AtPIP5K2-EYFP and NtRAC5-RFP are visible as bright dots at the cell surface. Scale bars, 10 µm. C, Representative median confocal frames extracted from the z-stack projection shown in (A) and representing the individual channels for AtPIP5K2-EYFP or NtRac5-RFP with heatmap colors, as indicated. Note that high intensity values from both channels localize in the same areas at the cell periphery. D, The sum intensities were determined for the vertical pixel columns of each channel (please refer to Supplementary Figure S5 and Materials and methods section for details). Upper panel, sum intensities for AtPIP5K2-YFP (green) and NtRac5-RFP (red). Lower panel, detail view if the region

compared to the growth of positive (+) and negative controls (−). The interaction was verified by an immuno pull down experiment (Figure 8G). For this purpose, both proteins were recombinantly expressed in *E. coli*, AtPIP5K2 as a fusion to an N-terminal maltose-binding protein (MBP) tag (MBP-AtPIP5K2); and NtRac5 as a fusion to an N-terminal glutathione S-transferase (GST) tag (GST-NtRac5). The GST protein was expressed as a negative control. Upon coincubation of either GST or GST-NtRac5 with MBP-AtPIP5K2, the MBP-AtPIP5K2 protein was only detected in the immunoprecipitate with GST-NtRac5, not in that with GST alone (Figure 8G). The immuno-pull down indicates that MBP-AtPIP5K2 bound to GST-NtRac5 but not to GST (Figure 8G) and suggests a direct physical interaction between the AtPIP5K2 and NtRac5 proteins.

A functional link between AtPIP5K2 and NtRac5 was addressed by monitoring the incidence of pollen tube tip swelling upon individual or the combined expression of these proteins or of relevant protein variants (Figure 8H). The coexpression of AtPIP5K2-EYFP with a CFP control in pollen tubes resulted in significant tip swelling, compared to control cells coexpressing CFP and EYFP, as indicated (Figure 8H). Similarly, the coexpression of a constitutive active (CA) variant of NtRac5, NtRac5 G15V-mCherry, with a CFP control also resulted in significant pollen tube tip swelling, as did the coexpression of AtPIP5K2-EYFP with NtRac5 G15V-mCherry, as indicated (Figure 8H). By contrast, no tip swelling was observed when a dominant negative (DN) variant of NtRac5, NtRac5 T20N-mCherry was expressed. Importantly, the expression of the DN NtRac5 T20N-mCherry abolished the effect of coexpressed AtPIP5K2-EYFP on pollen tube tip swelling (Figure 8H), indicating that activation of NtRac5 was required for the effect of AtPIP5K2 on pollen tube tip swelling. We conclude that NtRac5 and AtPIP5K2 act in a common pathway to mediate effects on actin and cause pollen tube tip swelling.

To further substantiate this important finding, we next used the coexpression approach to test for functional interplay of AtPIP5K2 with another element of ROP signaling, the pollen expressed tobacco guanidine nucleotide dissociation inhibitor, NtRhoGDI2 (Klahre et al., 2006; Ischebeck et al., 2011; Sun et al., 2015). NtRhoGDI2 can bind NtRac5 in the cytosol, thereby controlling the pool of NtRac5 that can be activated at the plasma membrane (Klahre et al., 2006; Sun et al., 2015). In previous work, it was proposed that PtdIns(4,5)P_2 can serve as a GDI-displacement factor (GDF; Faure et al., 1999) and that in pollen tubes PtdIns(4,5)P_2 may promote the release of NtRac5 from the NtGHDI2/NtRac5 complex (Kost, 2008; Ischebeck et al., 2011). AtPIP5K2-mediated pollen tube tip swelling might thus be explained at the molecular level by enhanced PtdIns(4,5)P_2 production promoting the release and activation of NtRac5 at the plasma membrane, with ensuing stabilizing effects on actin and tip swelling (Klahre et al., 2006; Ischebeck et al., 2011). When AtPIP5K2-EYFP was coexpressed with a CFP control, we observed significant tip swelling compared to control pollen tubes expressing EYFP and CFP (Figure 8I, as indicated), as in previous experiments. By contrast, decreasing degrees of pollen tube tip swelling were observed when AtPIP5K2-EYFP was coexpressed with NtRhoGDI2-RFP, using increasing amounts of the *NtRhoGDI2-RFP* cDNA for particle bombardment to achieve

Figure 8 (Continued)
of interest indicated by the box in the upper panel. E, Correlation analysis of sum intensity profiles obtained for AtPIP5K2-EYFP and NtRac5-RFP. Left panel, Representative correlation plot for the fluorescence distributions given in (D). The correlation is characterized by a high Pearson coefficient R of 0.95. Right panel, Pearson coefficients obtained accordingly from 11 correlation analyses, with a mean R of 0.87, indicating consistently high correlations between the spatial distributions of AtPIP5K2-EYFP and NtRac5-RFP. F, G, AtPIP5K2 and NtRac5 proteins were tested for interaction in a protein complex. F, Interaction of AtPIP5K2 and NtRac5 according to split-ubiquitin-based yeast-two-hybrid analysis. In this system, AtPIP5K2 is expressed as a fusion to an Ost4-membrane anchor, which attaches the fusion protein to the cytoplasmic face of the endoplasmic reticulum. Positive interaction of the protein partners is indicated by yeast growth on selective −LTH media compared to growth of the positive (+) and negative controls (−). Growth of all colonies on −LT media indicates the presence of the correct genotypes of the transformed yeast tested. The data are shown in triplicates and are representative for four biological experiments with similar results. G, Interaction of AtPIP5K2 and NtRac5 according to immuno pull-down experiments. The AtPIP5K2 and NtRac5 proteins were recombinantly expressed in *E. coli* as fusions to N-terminal GST or MBP tags, respectively. The GST-NtRac5 and MBP-AtPIP5K2 proteins were affinity-purified and used for the pull-down experiment. Purified GST protein alone served as a negative control. Positive interaction is indicated by the detection of full-length MBP-AtPIP5K2 upon immunoprecipitation with GST-NtRac5, but not with GST alone. The blots shown are representative for two experiments. H, I, Pollen tube tip swelling was used as a morphological marker to assess the functional interplay of AtPIP5K2 with elements of tobacco ROP signaling in vivo. H, Functional interplay between AtPIP5K2 and NtRac5. Pollen tube tip widths were determined upon the coexpression of the control proteins, CFP with EYFP; AtPIP5K2-EYFP with CFP; the constitutive active NtRac5 G15V-RFP with CFP; AtPIP5K2-EYFP with NtRac5 G15V-RFP; the dominant negative NtRac5 T20N-RFP with CFP; and AtPIP5K2-EYFP with NtRac5 T20N-RFP. Please note the absence of pollen tube tip swelling upon the coexpression of AtPIP5K2-EYFP together with NtRac5 T20N-RFP, indicating that activation of NtRac5 is required for the effect of AtPIP5K2-EYFP on tip swelling. Data are given as means ± standard deviation and represent measurements of ⩾100 transgenic pollen tubes. I, Functional interplay between AtPIP5K2 and NtRhoGDI2. Pollen tube tip widths were determined upon the coexpression of the control proteins, CFP with EYFP; AtPIP5K2-EYFP with CFP; NtRhoGDI2-RFP with CFP; and AtPIP5K2-EYFP with NtRhoGDI2-RFP. Numbers indicate the use of 2.5-μg or of 5-μg plasmid DNA for the biolistic transformation of pollen tubes to modulate the expression levels of NtRhoGDI2-RFP. Please note the reduced pollen tube tip swelling upon the coexpression of AtPIP5K2-EYFP together with increasing levels of NtRhoGDI2. Data are given as means ± standard deviation and represent measurements of ⩾100 transgenic pollen tubes. Letters indicate significant differences according to a one-way Anova test with Tukey post hoc analysis.

increasing expression levels. The data indicate that the coexpression of NtRhoGDI2-RFP canceled the effects of AtPIP5K2-EYFP, which is consistent with the previously proposed function of PtdIns(4,5)P_2 as a GDF. For the confidence intervals associated with the significance categories a, b, and c for data reported in Figure 8, H and I, please refer to Supplementary Table 1.

Together, the data provide evidence that AtPIP5K2 localizes in plasma membrane nanodomains of pollen tubes in close spatial proximity with NtRac5. AtPIP5K2 interacts physically with NtRac5, and both proteins act in a common pathway to effect pollen tube tip swelling, likely through a regulatory effect on pollen tube actin dynamics.

Discussion

In this study, we addressed subcompartmentalization as an aspect of localized functional specification of the plasma membrane, with a focus on membrane nanodomains containing the regulatory phospholipid, PtdIns(4,5)P_2. For the functional aspects of our study, we exploited the unique properties of the tobacco pollen tube model, where alternative functions of the PI4P 5-kinases AtPIP5K2 and NtPIP5K6 have previously been found to coexist within a narrow subapical region of the plasma membrane.

Nano-organization of PtdIns(4,5)P_2 in the pollen tube plasma membrane

The subcompartmentalization of plasma membrane proteins in membrane nanodomains — or possibly "rafts" (Simons and Toomre, 2000; Simons and Vaz, 2004) — has previously been proposed for plants based on the subcellular localization of fluorescent markers for proteins identified, e.g. by proteomic analysis of detergent-insoluble membrane (DIM) preparations (Mongrand et al., 2004), such as remorins (Morel et al., 2006). Fluorescent variants of such markers show clear association with membrane nanodomains when analyzed microscopically and have been used as markers for nanodomain structure and membrane organization in the context of physiological processes mostly related to pathogen infection (Lefebvre et al., 2007; Raffaele et al., 2007, 2009; Lefebvre et al., 2010; Jarsch and Ott, 2011; Marin and Ott, 2012; Toth et al., 2012; Bozkurt et al., 2014; Jarsch et al., 2014; Konrad et al., 2014; Bucherl et al., 2017; Liang et al., 2018). While previous studies have focused mainly on the nanodomain association of proteins, it is evident that membrane lipids will also be essential determinants of membrane nanodomain formation. Based on our SD imaging of the distribution of the PtdIns(4,5)P_2 biosensor, RedStar-PLC-PH, in the pollen tube plasma membrane, we observed the subcompartmentalization of the biosensor into nanodomains (Figure 2). This pattern is consistent with previous reports, for instance because PtdIns(4,5)P_2 has been proposed to be essential for the membrane insertion of nanodomain-associated remorins (Gronnier et al., 2017). Importantly, the nano-organization of PtdIns(4,5)P_2 in the pollen tube plasma membrane provides a rationale for coexisting alternative roles of PtdIns(4,5)P_2.

PtdIns(4,5)P_2-nanodomains influence ROP signaling

The comparison of the functionally divergent nanodomain-associated PI4P 5-kinases AtPIP5K2/NtPIP5K2 with NtPIP5K6 suggests that PtdIns(4,5)P_2 formed in nanodomains exerts a different effect than PtdIns(4,5)P_2 outside the domains (see Figures 1, 4). Specifically, actin stabilization and pollen tube tip swelling emerged as a consequence of PtdIns(4,5)P_2 formed in plasma membrane nanodomains defined by AtPIP5K2 or NtPIP5K2 (see Figures 1, 6, 7). PtdIns(4,5)P_2 has previously been proposed to mediate pollen tube tip swelling through effects on the actin cytoskeleton and by circumstantial evidence been linked to ROP signaling (Ischebeck et al., 2011). This notion is of particular interest, because Arabidopsis ROP6 has recently been found to associate with dynamic plasma membrane nanodomains (Platre et al., 2019). These ROP6 nanodomains were proposed to be sensitive to the abundance of phosphatidylserine (Platre et al., 2019), leading us to hypothesize that also other anionic lipids, such as PtdIns(4,5)P_2, might contribute to the nano-organization of ROPs. The effects of overexpressed AtPIP5K2-EYFP or NtPIP5K2-EYFP on in vivo actin distribution (Figure 6) and dynamics (Figure 7) in pollen tubes and the coordinated localization and physical interaction of AtPIP5K2 with the ROP, NtRac5 (Figure 8), are consistent with an effect of PtdIns(4,5)P_2 on ROP signaling and cytoskeletal control. Together with the finding that the catalytic activity of AtPIP5K2 was required for its effects on actin (Figure 7), the functional interplay of AtPIP5K2 with NtRac5 (Figure 8H) and NtRhoGDI2 (Figure 8I) provides experimental evidence that PtdIns(4,5)P_2 acts as a GDI displacement factor (GDF). This notion is consistent with previously proposed models (Kost, 2008) suggesting that as a GDF PtdIns(4,5)P_2 might mediate the enhanced release of NtRac5 from cytosolic GDIs to the plasma membrane for activation (Faure et al., 1999; Kost, 2008; Ischebeck et al., 2011).

PtdIns(4,5)P_2 and phosphatidylserine may influence different aspects of plasma membrane nano-organization

The nano-organization of the plasma membrane may enable interactions of PtdIns(4,5)P_2 or its downstream effectors, such as NtRac5, with specific partners, thus enabling divergent functional consequences, as outlined in the simplified model scheme (Figure 9). It appears plausible that plasma membrane nanodomains serve as platforms for proteins, such as PIP5K2 orthologs, and ROPs, such as NtRac5, which assemble into functional complexes to influence the membrane attachment and stabilization of actin filaments (Figure 9A). It is possible that the localized attachment of actin filaments to the plasma membrane also serves as an initiating factor for the assembly of proteins in membrane nanodomains, or that both nanodomains and actin exert mutual effects in a self-organizing manner. Within plasma

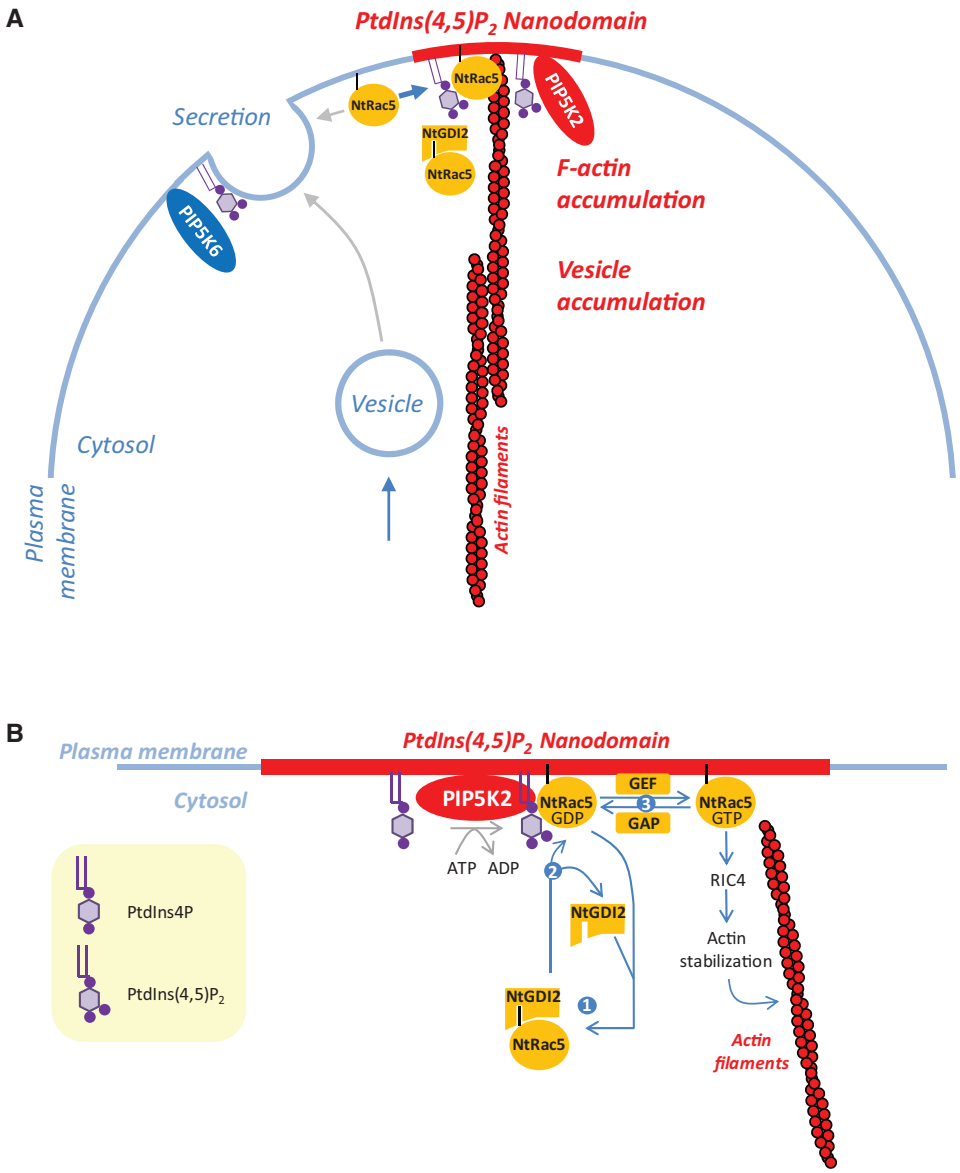

Figure 9 Model for the influence of nanodomain-associated PtdIns(4,5)P_2 and PIP5K2 orthologs on NtRac5 and actin dynamics. Polar tip growth of pollen tubes requires the close spatio-temporal coordination of actin dynamics and secretion/endocytosis. A, Nano-organization of the plasma membrane with PIP5K2 associating with nanodomains (red) and PIP5K6 distributing uniformly (blue) in the plasma membrane. PtdIns(4,5)P_2 formed by PIP5K2 orthologs in nanodomains may act to stabilize the actin cytoskeleton (red filaments) through functional interplay with elements of ROP signaling, such as NtRac5 or NtRhoGDI2 (NtGDI2). Upon the overproduction of PtdIns(4,5)P_2 in nanodomains, such as upon the overexpression of PIP5K2 orthologs, NtRac5-dependent effects might be shifted towards promoting F-actin accumulation (thick blue arrow), possibly at the expense of other functions (thin grey arrows). The diffusely localized PtdIns(4,5)P_2 formed by PIP5K6 serves a role in promoting secretion, as indicated. B, Proposed functional interplay of nanodomain-associated PtdIns(4,5)P_2 with ROP signaling. PtdIns(4,5)P_2 may act as a GDF on NtGDI2 to promote NtRac5-dependent stabilization of the actin cytoskeleton. A pool of plasma membrane-associated NtRac5 is in a dynamic equilibrium with cytosolic NtRac5 bound to NtGDI2 (point 1). PtdIns(4,5)P_2 formed by PIP5K2 in plasma membrane nanodomains might act as a GDF to destabilize cytosolic NtRhoGDI2/NtRac5 complexes (point 2), thereby releasing more NtRac5 to the plasma membrane. At the plasma membrane, NtRac5 can be activated by GEFs to NtRac5-GTP, which initiates a signaling cascade that stabilizes actin (point 3). Other explanations are possible. GAP, GTPase-activating protein; GEF, Guanidine nucleotide exchange factor; PtdIns4P, phosphatidylinositol 4-phosphate; PtdIns(4,5)P_2, phosphatidylinositol 4,5-bisphosphate; RIC, ROP-interactive CRIB-domain containing protein.

membrane nanodomains, PtdIns(4,5)P_2 might influence NtRac5 availability for activation (Figure 9B), whereas—in analogy to the situation reported for ROP6 in Arabidopsis (Platre et al., 2019)—phosphatidylserine might possibly influence the lateral distribution of NtRac5. ROPs exert their regulatory effects by signaling through Rho-interactive CRIB-domain containing (RIC) proteins (Gu et al., 2005; Lee et al., 2008). In particular, RIC proteins have been proposed to mediate the coordination of actin dynamics and secretion in pollen tubes (Lee et al., 2008), and our data suggest that the

overproduction of PtdIns(4,5)P_2 in membrane nanodomains may shift NtRac5 effects towards RIC4-dependend F-actin accumulation, whereas overproduction of PtdIns(4,5)P_2 outside of membrane nanodomains might favor RIC3-dependent depolymerization of F-actin and promote exocytosis. In this scenario, ensuing overactivation of NtRac5 might result in the stabilization of cortical actin in the pollen tube tip through tobacco RIC4 homologs, possibly resulting in reduced rates of secretion and vesicle accumulation (Lee et al., 2008). PtdIns(4,5)P_2 within or outside of membrane nanodomains may thus serve to direct NtRac5 towards different RICs, thereby aiding the coordination between actin dynamics and secretion during pollen tube growth. The combined data on plasma membrane nanodomains for PtdIns(4,5)P_2 and the PIP5K2 orthologs from Arabidopsis or tobacco indicate that spatial separation of PtdIns(4,5)P_2 populations is one reason for the functional distinction previously reported for AtPIP5K2 vs. other PI4P 5-kinases of subfamily B (Ischebeck et al., 2008, 2010b; Stenzel et al., 2012). Our data lead us to suggest functional specification of PI4P 5-kinases on different branches of the phylogenetic (sequence) relations for subfamily B (Supplemental Figure 1). AtPIP5K2 and NtPIP5K2 exert effects on actin dynamics (this study), which might be coordinated with the effects of PIP5K4/PIP5K5/PIP5K6 orthologs on membrane trafficking (Ischebeck et al., 2008, 2010b; Sousa et al., 2008; Zhao et al., 2010; Hempel et al., 2017; Menzel et al., 2019); and possibly also with the action of PIP5K7, PIP5K8, PIP5K9 orthologs, which may only be activated upon particular exogenous triggers (Zarza et al., 2020).

Plasma membrane nano-organization and limited lateral diffusion of PtdIns(4,5)P_2

It is important to note that the observed spatial distribution patterns of PtdIns(4,5)P_2 or PI4P 5-kinase isoforms can help to explain functional consequences of PtdIns(4,5)P_2-dependent processes for pollen tube growth only if we assume that spatially separated PtdIns(4,5)P_2 pools do not mix before their respective downstream effects have taken place. Thus, the observed patterns lead us to postulate limited lateral diffusion of PtdIns(4,5)P_2 molecules from their sites of biosynthesis, which are defined by the localization of the different PI4P 5-kinase isoforms, i.e. AtPIP5K2 or NtPIP5K2 in nanodomains vs. NtPIP5K6 or AtPIP5K5 in continuous membrane patterns. While this concept may oversimplify, it is consistent with current models of membrane organization and restricted lateral movement of membrane components (Arumugam et al., 2015; Destainville et al., 2016). Current models on the structure of membrane nanodomains are mostly based on the raft hypothesis (Rajendran and Simons, 2005) and assume that a complex mixture of membrane lipids, including sphingolipids, sterols, and phosphoinositides, may form a joint structure with specific biophysical properties (Anishkin and Kung, 2013), facilitating certain membrane functions while excluding others. In particular, the attachment of cytoskeletal strands to the plasma membrane may require a localized rigidification around the sites of anchorage (Anishkin and Kung, 2013). Nanodomain organization may also create biophysical barriers for the lateral diffusion of intrinsic membrane proteins as well as for membrane lipids, such as PtdIns(4,5)P_2 (Gerth et al., 2017b). Considering the raft hypothesis (Simons and Ikonen, 1997; Simons and Toomre, 2000; Simons and Vaz, 2004), the finding of PI4P 5-kinases, such as AtPIP5K2 or NtPIP5K2 and a PtdIns(4,5)P_2 reporter in plasma membrane nanodomains is consistent with the previous report of PI4P 5-kinase activity associated with detergent-resistant membrane (DIM) fractions prepared from plasma membrane from tobacco leaves (Furt et al., 2010). Of note, PI4P 5-kinase activity was previously reported to reside in DIM preparations as well as outside of DIMs of tobacco leaves or bright yellow 2 (BY-2) cells (Furt et al., 2010), supporting our data indicating PtdIns(4,5)P_2 production within and outside of plasma membrane nanodomains (Figures 2, 4). Formation of PtdIns(4,5)P_2 by different PI4P 5-kinase isoforms, such as AtPIP5K2/NtPIP5K2 within, or NtPIP5K6 outside of nanodomains may determine the downstream effects of PtdIns(4,5)P_2 possibly through binding to alternative protein partners, resulting in the control of different PtdIns(4,5)P_2-dependent processes (Figure 9A). Localization of the enzymes in membrane nanodomains may thus facilitate the interaction with partners involved in the control of the actin cytoskeleton, such as ROPs (Figure 9, B and C), and enable differential regulation of PtdIns(4,5)P_2 effects in different membrane areas.

While our data suggest a distinct regulatory function of PtdIns(4,5)P_2 in plasma membrane nanodomains, it appears likely that the "diffuse" PtdIns(4,5)P_2 outside of the nanodomains may also be further subcompartmentalized. Besides a distinction between PtdIns(4,5)P_2 pools based on spatial separation, which may or may not be detectable by microscopy, it is possible that diffusely localizing PI4P 5-kinases may display a patchy pattern of activated and inactivated states, resulting in islands of active PI4P 5-kinases within a population of possibly not activated proteins that is diffusely distributed. This hypothesis is based on recent reports that the type B PI4P 5-kinase AtPIP5K6 is regulated in its activity by the mitogen-activated protein kinase (MAPK) MPK6, and that MPK6-mediated phosphorylation does not impair membrane association of PIP5K6 (Hempel et al., 2017; Menzel et al., 2019).

PtdIns(4,5)P_2 nanodomains only in pollen tubes and other open questions

The pollen tube system used in this study holds several unique advantages, including high levels of PtdIns(4,5)P_2 (Supplemental Figure 6A) and the previous characterization of divergent functional effects of AtPIP5K2 and NtPIP5K6 on pollen tube morphology (Stenzel et al., 2012). In previous studies, a contribution of phosphoinositides to the regulation of important physiological processes has also been reported for the vegetative portion of plants. These studies describe roles for phosphoinositides in clathrin recruitment

(König et al., 2008b; Ischebeck et al., 2013); the polarization of auxin efflux carriers of the PIN-FORMED (PIN)-family (Mei et al., 2012; Ischebeck et al., 2013; Tejos et al., 2014), of D6P-kinases (Barbosa et al., 2016) and of BRX and PAX proteins (Marhava et al., 2020); the control of cytokinesis (Lin et al., 2019); cell wall deposition (Rodriguez-Villalon et al., 2015), and roles in membrane trafficking during plant pathogen interactions (Shimada et al., 2019; Qin et al., 2020; Rausche et al., 2020). These reports are consistent with the presence of PtdIns(4,5)P_2 in membrane nanodomains occupied by phosphoinositides; however, in Arabidopsis hypocotyl cells we detected such nanodomains by SD only upon application of salt (Supplemental Figure 6B), thus artificially increasing PtdIns(4,5)P_2 levels. As a chemical difference has previously been found between PtdIns(4,5)P_2 molecular species in resting and salt-stressed Arabidopsis plants (König et al., 2007, 2008b), the nature of the punctate signals seen in the hypocotyl cells only upon salt stress remains unclear. Therefore, it currently remains uncertain whether our data from the gametophytic pollen tube system can be transferred to sporophytic portions of the plant.

Our study also does not address a contribution of other lipid classes to the formation of PtdIns(4,5)P_2-containing plasma membrane foci, so it remains an open question whether or not the lipid raft concept may be applied to the nanodomains observed here. The previous observations that defects in the biosynthesis of sterols (Men et al., 2008), sphingolipids (Markham et al., 2011), or phosphoinositides (Mei et al., 2012; Ischebeck et al., 2013; Tejos et al., 2014) all result in similar mistrafficking of PIN proteins, are in favor of the notion that these lipids form a joint functional membrane structure underlying these effects in sporophytic tissues. An oxysterol-binding protein fused to a fluorescent reporter has previously been shown to decorate a patchy pattern in the subapical plasma membrane of pollen tubes (Skirpan et al., 2006). Furthermore, oxysterol-binding proteins from the yeast *Saccharomyces cerevisiae* contain PH-domains that specifically bind phosphoinositides (Roy and Levine, 2004; Fairn et al., 2007) and influence Rho-dependent cell polarization (Kozminski et al., 2006). In the absence of further direct evidence, however, the contribution of other lipid classes to the formation of membrane nanodomains enriched in PtdIns(4,5)P_2 remains to be analyzed. Future experiments will be directed towards further unraveling the nano-organization and chemical composition of plant plasma membrane nanodomains.

Materials and methods

Plant materials and growth conditions

Experiments were performed using material from *N. tabacum* (ecotype Samsun N). Plants for pollen production were grown in a greenhouse on soil at 21°C–26°C at ambient humidity in a long-day regime (16 h light, 8 h darkness) under semi-controlled light intensities. Pollen was collected from plants after 8–9 weeks of cultivation.

cDNA constructs

The assembly of plasmids encoding AtPIP5K2-EYFP, AtPIP5K2-mCherry, NtPIP5K6-EYFP, NtPIP5K6-mCherry, 2_swap6-EYFP, and 6swap2-EYFP was previously described (Stenzel et al., 2012). The cDNA encoding NtPIP5K2 was amplified from cDNA isolated from RNA from leaves from 3-week-old tobacco (*N. tabacum*) plants using the primer combination NtPIPK2_Asc_for 5′-ATGTGGCGCGCCATGCC TGAGACTTTGATATTATC-3′/NtPIPK2_Nhe_rev 5′-ATGT CCTGTCTTCGACAAAAATTCTGCCTATGAAATTC-3′. The amplicon was moved as an AscI/NheI-fragment into the vectors Lat52-YFP-pEntryA or Lat52-mCherry-pEntryA, respectively. To create these plasmids, the coding sequences for EYFP or mCherry were amplified with NheI/BamHI sites and cloned into the vector pEntryA. The tomato Lat52 promoter was amplified with Sfi1 sites from the pLATGW (Twell et al., 1990) and introduced in front of the EYFP or mCherry cassette. The RedStar-PLC-PH construct was assembled as previously described (Ischebeck et al., 2010b). The LifeAct-RFP cassette (Berepiki et al., 2010) in the pAL10 vector, kindly provided by Dr Stephan Seiler (University of Freiburg, Germany), was digested with SalI and NotI and transferred into the pEntryD vector. The tomato Lat52 promoter was amplified with Sfi1 sites from the pLATGW (Twell et al., 1990) and placed in front of the LifeAct-RFP cassette. For LifeAct-EYFP, RFP, was then replaced with EYFP. The mTalin-YFP construct was a kind gift of Prof. Dr. Benedikt Kost (University of Erlangen, Germany). For yeast two hybrid analysis, the cDNA of the *At*PIP5K2 bait protein was cloned into the plasmid *pBT3-C-OST4*. *pBT3-C-OST4* was produced by inserting the cDNA of OST4 (*yeast oligosaccharyl transferase 4*) into the *Xba*I site upstream of the multiple cloning site (mcs) of the original pBT3-C plasmid (Dualsystems Biotech AG, Zürich, Switzerland) as previously described (Möckli et al., 2007). The At*PIP5K2* cDNA was amplified with the primer combination At*PIP5K2-OST4-for* 5′-ATGCGGCCATTACGGCCAAATGATGCGTGAACCGCTT-3′/ AtPIP5K2-OST4-rev 5′-ATGCGGCCGAGGCGGCCTGCCGTC TTCGATGAAGATT-3′. The primers introduced an *Sfi*IA site upstream and an *Sfi*IB site downstream of the At*PIP5K2* sequence, and the PCR fragment was inserted directionally into the *Sfi*I sites of the *pBT3-C-OST4* vector. The cDNAs for the prey protein NtRac5 were amplified using the primer combination NtRac5-SfiIA-for 5′-ATGCGGCCATTACGGCCA TGAGTGCTTCAAGGTTTATC-3′/NtRac5-SfiIB-rev 5′-ATG CGGCCGAGGCGGCCTCACAATATCGAGCAGGATTTTT-3′ and moved as *Sfi*I fragments into the mcs of pPR3-N (Dualsystems Biotech AG, Zürich, Switzerland). For the immuno pull-down experiments, AtPIP5K2 was expressed as a fusion to an N-terminal MBP tag and NtRac5 as a fusion to an N-terminal GST tag. Constructs for *E. coli* expression were based on the plasmids *pMAL-c5G* (New England Biolabs) and *pGEX-6p-1* (Ge-Healthcare). The coding sequence for AtPIP5K2 was amplified from Arabidopsis leaf cDNA using the primer combinations AtPIP5K2-NotI-for 5′-ATGCGCGGC CGCATGATGCGTGAACCGCTTGT-3′/AtPIPK2-EcoRI-rev 5′-

ATGCGAATTCTTAGCCGTCTTCGATGAAGATTC-3′, as previously reported (Gerth et al., 2017a). The coding sequence for NtRac5 was amplified from tobacco (*N. tabacum*) pollen tube cDNA using the primer combination NtRac5-BamHI-for 5′-ATGCGGATCCATGAGTGCTTCAAGGTTTATC-3′/NtRac5-NotI-rev 5′-ATGCGCGGCCGCTCACAATATCGAGCAGGATTTTT-3′. The coding sequences were subsequently moved as *Not*I/*Eco*RI and *Bam*HI/*Not*I-fragments into the respective vector backbones.

Transient expression of constructs in tobacco pollen tubes

Mature pollen grains were collected from four to five tobacco flowers of approximately 8- to 9-week-old plants. Pollen were resuspended in liquid pollen tube growth media (Read et al., 1993) followed by the filtering of the pollen grains onto a cellulose acetate filter. Pollen were immediately transformed by bombardment with plasmid-coated 1-μm gold particles with a helium-driven particle accelerator (PDS-1000/He; Bio-Rad) using 1,350 psi rupture disks and a vacuum of 28 inches of mercury. Prior to the bombardment, these gold particles were coated with 4–5 μg of the desired plasmid of interest. After bombardment, the pollen grains were transferred into 300 μL of pollen tube growth media which was then equally divided onto three microscopy glass slides and viewed under the microscope 4–6 h after the bombardment. All bombardment experiments were performed in at least three independent biological experiments.

Live cell microscopy and image processing

Images were acquired with a Zeiss LSM880 Airyscan system or with a Zeiss Cell observer SD with a Yokogawa CSU-X1 spinning disc unit. For imaging with the LSM880, a 40× objective without immersion was used and images were captured with the ZEN Black image analysis software. During acquisition with the LSM880, EYFP was excited with a 514-nm laser line and imaged with a HFT 514-nm main beam splitter (MBS) while mCherry or RFP was excited with a 561-nm laser line and imaged with a HFT 561-nm MBS. The Zeiss Cell observer SD was used for acquiring z-stacks and time-lapse images of pollen tubes expressing EYFP or mCherry fluorophores, which were analyzed with the Zen Blue image analysis software. Images were acquired with a 63× oil immersion objective and captured with a Photometrics Evolve 512 Delta EM-CCD camera. EYFP was excited at 488 nm and mCherry, RFP or RedStar at 561 nm using 503–546 nm and 583–700 nm dual band emission filters (AHF Analysentechnik AG), respectively.

All images were processed using Fiji software (Schindelin et al., 2012). Nanodomain lifetimes were first acquired using the SD microscope where images were captured every 2 s over a period of 120 s. The images were then processed using the Fiji "Trackmate" plugin (Tinevez et al., 2017). With the same plugin, the x;y coordinates of nanodomains were extracted and the Euclidean distances from the tip measured (x;y coordinates of each pollen tube tip analyzed were manually extracted). For size determination of PtdIns(4,5)P_2 nanodomains, punctate signals were manually picked and listed into a ROI manager. To assess the intensity distributions of AtPIP5K2-EYFP, NtPIP5K6-EYFP, 2swap6-EYFP, and 6swap2-EYFP at the plasma membrane, the Fiji software was used. An area of 22 × 22 pixels at the cell surface of multiple pollen tubes was manually picked, listed into the ROI manager and the standard deviation among pixel values was calculated. High standard deviations reflect the presence of heterogeneous intensity distribution at the cell membrane, and therefore foci formation; by contrast, low standard deviations reflect a uniform distribution of intensities, and therefore diffuse distribution of the marker.

For correlation analysis of AtPIP5K2-EYFP with RedStar-PLC-PH and of AtPIP5K2-EYXFP with NtRac5-RFP, multiple pollen tubes were analyzed, each with five z-stacks of 0.3-μm slices. For each image, fluorescence channels (green and red) were split and individually analyzed. Pixel intensities were extracted using Fiji; every image was then divided into longitudinal sections of 1-pixel width, and the intensity values of each pixel column was summed up and plotted as a function of space. The product momentum Pearson correlation coefficient (R) among the two channels was then determined (please also see Supplementary Figure 5).

Actin occupancy was determined using the pixel classification and object classification tool from the machine-learning software Ilastik (Berg et al., 2019). Pixel occupancy of LifeAct fluorescence signal of each pollen tube was extracted and divided by the area of the pollen tube tip, and values were converted into area percentages. To determine the ratio of plasma membrane vs. cytosolic fluorescences, the same software tool was used to extract the signal intensities from imaging frames.

Actin dynamics were monitored over time in full z-stacks of 2-μm slices from pollen tubes transiently transformed with mTalin-YFP, with image acquisition at every 10 s over a period of 5 min (resulting in 30 frames), using LSM. Kymographs were then extracted for every pollen tube using Fiji software. In particular, to focus on actin dynamics in the pollen tube tip, for every image an area of 28 × 25 micron at the tip was cropped and analyzed. Kymograph data were recorded at the center of the tube. Dynamic actin structures are apparent by this analysis as short and/or asymmetric fluorescence signals in the kymograph. By contrast, stabilized/static actin structures appear in the kymographs as long fluorescence lines. Fluorescence signals from each kymograph were segmented and analyzed using the pixel classification and object classification tool from Ilastik software (Berg et al., 2019). The lengths of each fluorescence signal were extracted in pixels (Euclidean diameter). Fluorescence signals shorter than 5 pixels were considered as noise and were excluded from measurements.

For pectin staining pollen tubes were stained as previously reported (Iwai et al., 2006; Ischebeck et al., 2008) with ruthenium red (Sigma-Aldrich) using a final concentration of 0.01% (w/v) and imaged using a light microscope (Zeiss Axiovert 200) within 5–15 min after addition of the dye.

For staining with FM 4-64 or FM 1-43 (both Molecular Imaging Products), the dyes were diluted to a working concentration of 2.5 μM and added to pollen tubes on glass slides 2–3 min before imaging. For staining with Di-4-ANEPPDHQ (Thermo Fisher Scientific) the dye was diluted to a working concentration of 1 μM and added to pollen tubes on glass slides 2–3 min before imaging.

Recombinant protein expression

Extracts containing recombinant protein were generated by expression in *E. coli* Rosetta 2 cells. MBP-AtPIP5K2 was expressed and enriched exactly as previously described (Dejonghe et al., 2016). For recombinant expression of NtRac5, *pGEX6p-1-NtRac5* was transformed into Rosetta 2 expression cells. Cells were grown in liquid LB media selecting for carbenicillin resistance. Expression cultures of 300 mL were incubated at 37°C with shaking at 200 rpm. Expression was induced at an optical density of 0.8 by adding 0.1 mM isopropyl-β-D-thiogalactosylpyranoside (IPTG). Cultures were incubated overnight at 18°C with shaking at 200 rpm and harvested by centrifugation (3,000*g* for 15 min at 4°C). The cell sediment was resuspended on ice in lysis buffer containing 50-mM Tris-HCl, pH 8, 150-mM NaCl, 1-mM EDTA, and 50 U of lysozyme. Cells were ruptured by ultrasound on ice, using five 60 s bursts in a Sonifier Cell Disruptor B15 (Branson Dietzenbach, Germany) at 50% power and 50% impulse settings. The protein extracts were cleared by centrifugation (15,000*g* for 10 min at 4°C) and stored at −80°C.

Protein interaction studies

The split-ubiquitin-based yeast two-hybrid-system (Dualsystems Biotech, Zürich, Switzerland (Johnsson and Varshavsky, 1994)) was used to analyze protein–protein interactions between NtRac5 and AtPIP5K2 as bait, which was expressed as a fusion to an N-terminal OST4-anchor (Möckli et al., 2007). All analyses were performed according to the manufacturer's instructions. For immuno-pull-down experiments, recombinant GST, GST-NtRac5 were immobilized on glutathione-agarose (Thermo Fisher Scientific) and incubated with purified recombinant MBP-AtPIP5K2 protein for 60 min at 4°C. Upon washing of the resin, GST-bound proteins were eluted with 50-mM glutathione. Interacting MBP-AtPIP5K2 protein was detected using an anti-MBP antibody (New England Biolabs, cat# E8032S) used at a dilution of 1:10,000 in 1× TBS buffer (20-mM Tris, pH 7.5, 150-mM NaCl) containing 3% (w/w) milk powder (Serva). Protein input was detected using an anti-GST antibody (Sigma, cat# 27457701V) used at a dilution of 1:2,000 in 1× TBS buffer containing 3% (w/w) milk powder (Serva).

Extraction, enrichment and quantitative analysis of PtdIns(4,5)P_2

The levels of unlabeled phosphoinositides were analyzed in different plant tissues by solid-phase adsorption chromatography and subsequent quantification via thin-layer and gas chromatography, as previously described (Launhardt et al., 2021). Material for the analysis was collected from rosette leaves from 21-day-old Arabidopsis plants; from leaves from 2-month-old tobacco (*N. tabacum*) plants; from pollen grains harvested from 50 tobacco (*N. tabacum*) flowers; or from pollen tubes harvested from 50 tobacco (*N. tabacum*) flowers and incubated for 3.5 h in liquid pollen media (Ischebeck et al., 2008). In brief, the plant material was ground in liquid N_2 and lipid extraction was performed as described in (König et al., 2008a). For enrichment of phospholipids, solid-phase extraction columns (Agilent Technologies) were used and lipid classes were subsequently eluted by using 5 mL of the following solvents for each fraction: neutral lipids – $CHCl_3$ (v/v); galactolipids – acetone:-methanol (9:1, v/v); phospholipids – methanol:acetic acid (10:0.1, v/v). The phospholipid fraction was reextracted by adding 5 mL each of $CHCl_3$ and H_2O, and the organic phases were collected. Subsequently PtdIns(4,5)P_2 was determined as previously described (König et al., 2008a).

Phylogenetic analysis

Phylogenetic analysis was based on amino acid sequences aligned using MAFFT multiple sequence alignment software with the L-INS-i option (Katoh et al., 2005). Alignments were manually edited and ProtTest 3.0 was used to select the best-fit model of protein evolution (Abascal et al., 2005). The alignment used for analysis is provided in Supplemental Data Set 1. Phylogenetic relationships of the amino acid sequences were inferred using the maximum likelihood method implemented in MEGA 5 (JTT + G + F, 1000 bootstrap replicates) as previously described (Tamura et al., 2011). The resulting dendrogram was mid-point rooted and edited with iTOL (https://itol.embl.de/).

Statistical evaluation

All quantitative data were tested for statistical significance using two-tailed Student's *t* test. Confidence intervals are given in the figure legends for each data set. Confidence intervals are reported in the respective figure legends and for data in Figure 8, H and I in Supplemental Table 1. Data were plotted using GraphPad Prism version 8 and BoxPlotR (http://shiny.chemgrid.org/boxplotr/; Spitzer et al., 2014).

Accession numbers

Sequence data from this article can be found in the GenBank/EMBL data libraries under the following accession numbers: AtPIP5K2, At1g77740; AtPIP5K5, At2g41210; NtPIP5K2, XM_016631252; NtPIP5K6, XM_016599345; NtRac5, AJ250174; NtRhoGDI2, DQ416769.

Supplemental data

The following materials are available in the online version of this article.

Supplemental Figure 1. Phylogenetic relations of plant PI4P 5-kinases, including AtPIP5K2, NtPIP5K2 and NtPIP5K6, used in this study.

Supplemental Figure 2. Influence of expressed fluorescence markers on pollen tube growth rates.

Supplemental Figure 3. Diffuse localization of AtPIP5K5-EYFP, a PI4P 5-kinase promoting apical pectin secretion in pollen tubes.

Supplemental Figure 4. Alignment of red and green fluorescence detection in the LSM setup used.

Supplemental Figure 5. Analytic work flow for the analysis of fluorescence intensity distributions of irregularly-shape structures by extracting vertical pixel columns and determining the sum intensities.

Supplemental Figure 6. Analysis of PtdIns(4,5)P_2 in different plant tissues.

Supplemental Table 1. Confidence intervals for the significance categories a, b and c for data presented in Fig. 8 H and I.

Supplemental Data Set 1. Alignments used to generate the phylogeny presented in Supplemental Figure 1.

Supplemental Movie 1. The PtdIns(4,5)P_2-specific biosensor RedStar-PLC-PH decorates plasma membrane nanodomains in tobacco pollen tubes.

Supplemental Movie 2. The PtdIns(4,5)P_2-specific biosensor RedStar-PLC-PH decorates plasma membrane nanodomains in tobacco pollen tubes.

Supplemental Movie 3. Bright field imaging of a growing tobacco pollen tube transformed with RedStar-PLC-PH.

Supplemental Movie 4. Dynamic fluorescent plasma membrane nanodomains in a growing pollen tobacco pollen tube expressing RedStar-PLC-PH.

Supplemental Movie 5. Bright field imaging of a non-growing tobacco pollen tube transformed with RedStar-PLC-PH.

Supplemental Movie 6. Dynamic fluorescent plasma membrane nanodomains in a non-growing pollen tobacco pollen tube expressing RedStar-PLC-PH.

Supplemental Movie 7. Bright field imaging of a tobacco pollen tube expressing AtPIP5K2-EYFP.

Supplemental Movie 8. Dynamic fluorescent plasma membrane nanodomains in a tobacco pollen tube expressing AtPIP5K2-EYFP.

Supplemental Movie 9. Dynamic fluorescent plasma membrane nanodomains in a tobacco pollen tube expressing AtPIP5K2 K470A-EYFP.

Supplemental Movie 10. Dynamic fluorescent plasma membrane nanodomains in a tobacco pollen tube expressing NtPIP5K2-EYFP.

Supplemental Movie 11. Actin dynamics in a growing tobacco pollen tube coexpressing mCherry and mTalin-YFP.

Supplemental Movie 12. Actin dynamics in a non-growing tobacco pollen tube coexpressing mCherry and mTalin-YFP.

Supplemental Movie 13. Actin dynamics in a pollen tube coexpressing AtPIP5K2-mCherry and mTalin-YFP.

Supplemental Movie 14. Actin dynamics in a growing pollen tube coexpressing AtPIP5K2 K470A-mCherry and mTalin-YFP.

Supplemental Movie 15. Actin dynamics in a non-growing pollen tube coexpressing AtPIP5K2 K470A-mCherry and mTalin-YFP.

Supplemental Movie 16. Actin dynamics in a pollen tube coexpressing NtPIP5K2-mCherry and mTalin-YFP.

Supplemental Movie 17. Actin dynamics in a growing pollen tube coexpressing NtPIP5K6-mCherry and mTalin-YFP.

Supplemental Movie 18. Actin dynamics in a non-growing pollen tube coexpressing NtPIP5K6-mCherry and mTalin-YFP.

Supplemental Movie Legends.

Acknowledgments

cDNA clones for mTalin, NtRac5, NtRac5 G15V, NtRac5 T20N, and NtRhoGDI2, were kindly provided by Prof. Dr Benedikt Kost (University of Erlangen, Germany). The cDNA encoding LifeAct was a kind gift of Dr Stephan Seiler (University of Freiburg, Germany).

Funding

Financial support by the German Research Foundation (DFG, grant nos. He3424/1-1, He3424/6-1, He3424/6-2, CRC648 TP B10, INST271/371-1 FUGG and 400681449/GRK2498 TP01 to I.H.) is gratefully acknowledged.

Conflict of interest statement. None declared.

References

Arumugam S, Petrov EP, Schwille P (2015) Cytoskeletal pinning controls phase separation in multicomponent lipid membranes. Biophys J **108**: 1104–1113

Balla T, Varnai P (2002) Visualizing cellular phosphoinositide pools with GFP-fused protein-modules. Sci STKE **2002**: PL3

Barbosa IC, Shikata H, Zourelidou M, Heilmann M, Heilmann I, Schwechheimer C (2016) Phospholipid composition and a polybasic motif determine D6 PROTEIN KINASE polar association with the plasma membrane and tropic responses. Development **143**: 4687–4700

Bashline L, Li S, Zhu X, Gu Y (2015) The TWD40-2 protein and the AP2 complex cooperate in the clathrin-mediated endocytosis of cellulose synthase to regulate cellulose biosynthesis. Proc Natl Acad Sci USA **112**: 12870–12875

Berepiki A, Lichius A, Shoji JY, Tilsner J, Read ND (2010) F-actin dynamics in Neurospora crassa. Eukaryot Cell **9**: 547–557

Berg S, Kutra D, Kroeger T, Straehle CN, Kausler BX, Haubold C, Schiegg M, Ales J, Beier T, Rudy M, et al. (2019) ilastik: interactive machine learning for (bio)image analysis. Nat Methods **16**: 1226–1232

Bloch D, Pleskot R, Pejchar P, Potocký M, Trpkošová P, Cwiklik L, Vukašinović N, Sternberg H, Yalovsky S, Žárský V (2016) Exocyst SEC3 and phosphoinositides define sites of exocytosis in pollen tube initiation and growth. Plant Physiol **172**: 980–1002 10.1104/pp.16.00690 27516531

Bozkurt TO, Richardson A, Dagdas YF, Mongrand S, Kamoun S, Raffaele S (2014) The plant membrane-associated REMORIN1.3 accumulates in discrete perihaustorial domains and enhances susceptibility to *Phytophthora infestans*. Plant Physiol **165**: 1005–1018

Bucherl CA, Jarsch IK, Schudoma C, Segonzac C, Mbengue M, Robatzek S, MacLean D, Ott T, Zipfel C (2017) Plant immune and

growth receptors share common signalling components but localise to distinct plasma membrane nanodomains. eLife **6**: e25114

Cheung AY, Wu HM (2008) Structural and signaling networks for the polar cell growth machinery in pollen tubes. Annu Rev Plant Biol **59**: 547–572

Dejonghe W, Kuenen S, Mylle E, Vasileva M, Keech O, Viotti C, Swerts J, Fendrych M, Ortiz-Morea FA, Mishev K, et al. (2016) Mitochondrial uncouplers inhibit clathrin-mediated endocytosis largely through cytoplasmic acidification. Nat Commun **7**: 11710

Destainville N, Schmidt TH, Lang T (2016) Where biology meets physics–a converging view on membrane microdomain dynamics. Curr Top Membr **77**: 27–65

Fairn GD, Curwin AJ, Stefan CJ, McMaster CR (2007) The oxysterol binding protein Kes1p regulates Golgi apparatus phosphatidylinositol-4-phosphate function. Proc Natl Acad Sci USA **104**: 15352–15357

Faure J, Vignais PV, Dagher MC (1999) Phosphoinositide-dependent activation of Rho A involves partial opening of the RhoA/Rho-GDI complex. Eur J Biochem **262**: 879–889

Fu Y, Wu G, Yang Z (2001) Rop GTPase-dependent dynamics of tip-localized F-actin controls tip growth in pollen tubes. J Cell Biol **152**: 1019–1032

Furt F, Simon-Plas F, Mongrand S (2011) Lipids of the plant plasma membrane. *In* **AS Murphy, W Peer, B Schulz**, eds, The Plant Plasma Membrane. Springer, Berlin, Germany, pp. 3–30

Furt F, Konig S, Bessoule JJ, Sargueil F, Zallot R, Stanislas T, Noirot E, Lherminier J, Simon-Plas F, Heilmann I, et al. (2010) Polyphosphoinositides are enriched in plant membrane rafts and form microdomains in the plasma membrane. Plant Physiol **152**: 2173–2187

Gadeyne A, Sánchez-Rodríguez C, Vanneste S, Di Rubbo S, Zauber H, Vanneste K, Van Leene J, De Winne N, Eeckhout D, Persiau G, et al. (2014) The TPLATE adaptor complex drives clathrin-mediated endocytosis in plants. Cell **156**: 691–704

Gerth K, Lin F, Daamen F, Menzel W, Heinrich F, Heilmann M (2017a) Arabidopsis phosphatidylinositol 4-phosphate 5-kinase 2 contains a functional nuclear localization sequence and interacts with alpha-importins. Plant J **92**: 862–878

Gerth K, Lin F, Menzel W, Krishnamoorthy P, Stenzel I, Heilmann M, Heilmann I (2017b) Guilt by association: a phenotype-based view of the plant phosphoinositide network. Annu Rev Plant Biol **68**: 349–374

Grebnev G, Ntefidou M Kost B (2017) Secretion and endocytosis in pollen tubes: models of tip growth in the spot light. Front Plant Sci **8**: 154

Gronnier J, Crowet JM, Habenstein B, Nasir MN, Bayle V, Hosy E, Platre MP, Gouguet P, Raffaele S, Martinez D, et al. (2017) Structural basis for plant plasma membrane protein dynamics and organization into functional nanodomains. eLife **6**: e26404

Gu Y, Fu Y, Dowd P, Li S, Vernoud V, Gilroy S, Yang Z (2005) A Rho family GTPase controls actin dynamics and tip growth via two counteracting downstream pathways in pollen tubes. J Cell Biol **169**: 127–138

Guo J, Yang Z (2020) Exocytosis and endocytosis: coordinating and fine-tuning the polar tip growth domain in pollen tubes. J Exp Bot **71**: 2428–2438

Heilmann I (2016) Phosphoinositide signaling in plant development. Development **143**: 2044–2055

Heilmann I, Ischebeck T (2016) Male functions and malfunctions: the impact of phosphoinositides on pollen development and pollen tube growth. Plant Reprod **29**: 3–20

Heilmann M, Heilmann I (2013) Arranged marriage in lipid signalling? The limited choices of PtdIns(4,5)P in finding the right partner. Plant Biol (Stuttg) **15**: 789–797

Heilmann M, Heilmann I (2015) Plant phosphoinositides-complex networks controlling growth and adaptation. Biochim Biophys Acta **1851**: 759–769

Hempel F, Stenzel I, Heilmann M, Krishnamoorthy P, Menzel W, Golbik R, Helm S, Dobritzsch D, Baginsky S, Lee J, et al. (2017) MAPKs influence pollen tube growth by controlling the formation of phosphatidylinositol 4,5-bisphosphate in an apical plasma membrane domain. Plant Cell **29**: 3030–3050

Hepler PK, Winship LJ (2015) The pollen tube clear zone: clues to the mechanism of polarized growth. J Integr Plant Biol **57**: 79–92

Ischebeck T, Stenzel I, Heilmann I (2008) Type B phosphatidylinositol-4-phosphate 5-kinases mediate pollen tube growth in *Nicotiana tabacum* and *Arabidopsis* by regulating apical pectin secretion. Plant Cell **20**: 3312–3330

Ischebeck T, Seiler S, Heilmann I (2010a) At the poles across kingdoms: phosphoinositides and polar tip growth. Protoplasma **240**: 13–31

Ischebeck T, Vu LH, Jin X, Stenzel I, Löfke C, Heilmann I (2010b) Functional cooperativity of enzymes of phosphoinositide conversion according to synergistic effects on pectin secretion in tobacco pollen tubes. Mol Plant **3**: 870–881

Ischebeck T, Stenzel I, Hempel F, Jin X, Mosblech A, Heilmann I (2011) Phosphatidylinositol-4,5-bisphosphate influences Nt-Rac5-mediated cell expansion in pollen tubes of Nicotiana tabacum. Plant J **65**: 453–468

Ischebeck T, Werner S, Krishnamoorthy P, Lerche J, Meijon M, Stenzel I, Löfke C, Wiessner T, Im YJ, Perera IY, et al. (2013) Phosphatidylinositol 4,5-bisphosphate influences PIN polarization by controlling clathrin-mediated membrane trafficking in Arabidopsis. Plant Cell **25**: 4894–4911

Iwai H, Hokura A, Oishi M, Chida H, Ishii T, Sakai S, Satoh S (2006) The gene responsible for borate cross-linking of pectin Rhamnogalacturonan-II is required for plant reproductive tissue development and fertilization. Proc Natl Acad Sci USA **103**: 16592–16597

Jaillais Y, Ott T (2020) The nanoscale organization of the plasma membrane and its importance in signaling: a proteolipid perspective. Plant Physiol **182**: 1682–1696

Jarsch IK, Ott T (2011) Perspectives on remorin proteins, membrane rafts, and their role during plant-microbe interactions. Mol Plant Microbe Interact **24**: 7–12

Jarsch IK, Konrad SS, Stratil TF, Urbanus SL, Szymanski W, Braun P, Braun KH, Ott T (2014) Plasma membranes are subcompartmentalized into a plethora of coexisting and diverse microdomains in Arabidopsis and Nicotiana benthamiana. Plant Cell **26**: 1698–1711

Johnson A, Vert G (2017) Single event resolution of plant plasma membrane protein endocytosis by TIRF microscopy. Front Plant Sci **8**: 612

Johnsson N, Varshavsky A (1994) Split ubiquitin as a sensor of protein interactions in vivo. Proc Natl Acad Sci USA **91**: 10340–10344

Kalmbach L, Hematy K, De Bellis D, Barberon M, Fujita S, Ursache R, Daraspe J, Geldner N (2017) Transient cell-specific EXO70A1 activity in the CASP domain and Casparian strip localization. Nat Plants **3**: 17058

Katoh K, Kuma K, Toh H, Miyata T (2005) MAFFT version 5: improvement in accuracy of multiple sequence alignment. Nucleic Acids Res **33**: 511–518

Klahre U, Kost B (2006) Tobacco RhoGTPase ACTIVATING PROTEIN1 spatially restricts signaling of RAC/Rop to the apex of pollen tubes. Plant Cell **18**: 3033–3046

Klahre U, Becker C, Schmitt AC, Kost B (2006) Nt-RhoGDI2 regulates Rac/Rop signaling and polar cell growth in tobacco pollen tubes. Plant J **46**: 1018–1031

König S, Mosblech A, Heilmann I (2007) Stress-inducible and constitutive phosphoinositide pools have distinct fatty acid patterns in *Arabidopsis thaliana*. FASEB J **21**: 1958–1967

König S, Hoffmann M, Mosblech A, Heilmann I (2008a) Determination of content and fatty acid composition of unlabeled phosphoinositide species by thin layer chromatography and gas chromatography. Anal Biochem **378**: 197–201

König S, Ischebeck T, Lerche J, Stenzel I, Heilmann I (2008b) Salt stress-induced association of phosphatidylinositol-4,5-bisphosphate with clathrin-coated vesicles in plants. Biochem J **415**: 387–399

Konopka CA, Backues SK, Bednarek SY (2008) Dynamics of Arabidopsis dynamin-related protein 1C and a clathrin light chain at the plasma membrane. Plant Cell **20**: 1363–1380

Konrad SS, Popp C, Stratil TF, Jarsch IK, Thallmair V, Folgmann J, Marin M, Ott T (2014) S-acylation anchors remorin proteins to the plasma membrane but does not primarily determine their localization in membrane microdomains. New Phytol **203**: 758–769

Kost B (2008) Spatial control of Rho (Rac-Rop) signaling in tip-growing plant cells. Trends Cell Biol **18**: 119–127

Kost B, Spielhofer P, Chua NH (1998) A GFP-mouse talin fusion protein labels plant actin filaments in vivo and visualizes the actin cytoskeleton in growing pollen tubes. Plant J **16**: 393–401

Kost B, Lemichez E, Spielhofer P, Hong Y, Tolias K, Carpenter C, Chua NH (1999) Rac homologues and compartmentalized phosphatidylinositol 4, 5-bisphosphate act in a common pathway to regulate polar pollen tube growth. J Cell Biol **145**: 317–330

Kozminski KG, Alfaro G, Dighe S, Beh CT (2006) Homologues of oxysterol-binding proteins affect Cdc42p- and Rho1p-mediated cell polarization in Saccharomyces cerevisiae. Traffic **7**: 1224–1242

Kusano H, Testerink C, Vermeer JEM, Tsuge T, Shimada H, Oka A, Munnik T, Aoyama T (2008) The *Arabidopsis* phosphatidylinositol phosphate 5-kinase PIP5K3 is a key regulator of root hair tip growth. Plant Cell **20**: 367–380

Launhardt L, Matzner M, Heilmann M, Heilmann I (2021) Analysis of phosphoinositides from complex plant samples by solid-phase adsorption chromatography and subsequent quantification via thin-layer and gas chromatography. Methods Mol Biol (in press), Doi: 10.1007/978-1-0716-1362-7_21

Lee YJ, Szumlanski A, Nielsen E, Yang Z (2008) Rho-GTPase-dependent filamentous actin dynamics coordinate vesicle targeting and exocytosis during tip growth. J Cell Biol **181**: 1155–1168

Lefebvre B, Furt F, Hartmann MA, Michaelson LV, Carde JP, Sargueil-Boiron F, Rossignol M, Napier JA, Cullimore J, Bessoule JJ, et al. (2007) Characterization of lipid rafts from Medicago truncatula root plasma membranes: a proteomic study reveals the presence of a raft-associated redox system. Plant Physiol **144**: 402–418

Lefebvre B, Timmers T, Mbengue M, Moreau S, Herve C, Toth K, Bittencourt-Silvestre J, Klaus D, Deslandes L, Godiard L, et al. (2010) A remorin protein interacts with symbiotic receptors and regulates bacterial infection. Proc Natl Acad Sci USA **107**: 2343–2348

Li S, Chen M, Yu D, Ren S, Sun S, Liu L, Ketelaar T, Emons AM, Liu CM (2013) EXO70A1-mediated vesicle trafficking is critical for tracheary element development in Arabidopsis. Plant Cell **25**: 1774–1786

Liang P, Stratil TF, Popp C, Marin M, Folgmann J, Mysore KS, Wen J, Ott T (2018) Symbiotic root infections in Medicago truncatula require remorin-mediated receptor stabilization in membrane nanodomains. Proc Natl Acad Sci USA **115**: 5289–5294

Lichius A, Read ND (2010) A versatile set of Lifeact-RFP expression plasmids for live-cell imaging of F-actin in filamentous fungi. Fungal Genet Rep **57**: 8–14

Lin F, Krishnamoorthy P, Schubert V, Hause G, Heilmann M, Heilmann I (2019) A dual role for cell plate-associated PI4Kbeta in endocytosis and phragmoplast dynamics during plant somatic cytokinesis. EMBO J **38**: e100303

Mähs A, Ischebeck T, Heilig Y, Stenzel I, Hempel F, Seiler S, Heilmann I (2012) The essential phosphoinositide kinase MSS-4 is required for polar hyphal morphogenesis, localizing to sites of growth and cell fusion in *Neurospora crassa*. PLoS One **7**: e51454

Malho R, Liu Q, Monteiro D, Rato C, Camacho L, Dinis A (2006) Signalling pathways in pollen germination and tube growth. Protoplasma **228**: 21–30

Mamode Cassim A, Gouguet P, Gronnier J, Laurent N, Germain V, Grison M, Boutte Y, Gerbeau-Pissot P, Simon-Plas F, Mongrand S (2019) Plant lipids: Key players of plasma membrane organization and function. Prog Lipid Res **73**: 1–27

Marhava P, Aliaga Fandino AC, Koh SWH, Jelinkova A, Kolb M, Janacek DP, Breda AS, Cattaneo P, Hammes UZ, Petrasek J, et al. (2020) Plasma membrane domain patterning and self-reinforcing polarity in Arabidopsis. Dev Cell **52**: 223–235

Marin M, Ott T (2012) Phosphorylation of intrinsically disordered regions in remorin proteins. Front Plant Sci **3**: 86

Markham JE, Molino D, Gissot L, Bellec Y, Hematy K, Marion J, Belcram K, Palauqui JC, Satiat-Jeunemaitre B, Faure JD (2011) Sphingolipids containing very-long-chain fatty acids define a secretory pathway for specific polar plasma membrane protein targeting in Arabidopsis. Plant Cell **23**: 2362–2378

Mei Y, Jia WJ, Chu YJ, Xue HW (2012) Arabidopsis phosphatidylinositol monophosphate 5-kinase 2 is involved in root gravitropism through regulation of polar auxin transport by affecting the cycling of PIN proteins. Cell Res **22**: 581–597

Men S, Boutte Y, Ikeda Y, Li X, Palme K, Stierhof YD, Hartmann MA, Moritz T, Grebe M (2008) Sterol-dependent endocytosis mediates post-cytokinetic acquisition of PIN2 auxin efflux carrier polarity. Nat Cell Biol **10**: 237–244

Menzel W, Stenzel I, Helbig LM, Krishnamoorthy P, Neumann S, Eschen-Lippold L, Heilmann M, Lee J, Heilmann I (2019) A PAMP-triggered MAPK cascade inhibits phosphatidylinositol 4,5-bisphosphate production by PIP5K6 in Arabidopsis thaliana. New Phytol **224**: 833–847

Möckli N, Deplazes A, Hassa PO, Zhang Z, Peter M, Hottiger MO, Stagljar I, Auerbach D (2007) Yeast split-ubiquitin-based cytosolic screening system to detect interactions between transcriptionally active proteins. Biotechniques **42**: 725–730

Mongrand S, Morel J, Laroche J, Claverol S, Carde JP, Hartmann MA, Bonneu M, Simon-Plas F, Lessire R, Bessoule JJ (2004) Lipid rafts in higher plant cells: purification and characterization of Triton X-100-insoluble microdomains from tobacco plasma membrane. J Biol Chem **279**: 36277–36286

Monteiro D, Castanho Coelho P, Rodrigues C, Camacho L, Quader H, Malho R (2005a) Modulation of endocytosis in pollen tube growth by phosphoinositides and phospholipids. Protoplasma **226**: 31–38

Monteiro D, Liu Q, Lisboa F, Scherer GE, Quader H, Malhó R (2005b) Phosphoinositides and phosphatidic acid regulate pollen tube growth and reorientation through modulation of [Ca2 +]c and membrane secretion. J Exp Bot **56**: 1665–1674

Morel J, Claverol S, Mongrand S, Furt F, Fromentin J, Bessoule JJ, Blein JP, Simon-Plas F (2006) Proteomics of plant detergent resistant membranes. Mol Cell Proteomics **5**: 1396–1411

Mueller-Roeber B, Pical C (2002) Inositol phospholipid metabolism in *Arabidopsis*. Characterized and putative isoforms of inositol phospholipid kinase and phosphoinositide-specific phospholipase C. Plant Physiol **130**: 22–46

Noack LC, Jaillais Y (2020) Functions of anionic lipids in plants. Annu Rev Plant Biol **71**: 71–102

Orr RG, Cheng X, Vidali L, Bezanilla M (2020) Orchestrating cell morphology from the inside out - using polarized cell expansion in plants as a model. Curr Opin Cell Biol **62**: 46–53

Platre MP, Bayle V, Armengot L, Bareille J, Marques-Bueno MDM, Creff A, Maneta-Peyret L, Fiche JB, Nollmann M, Miege C, et al. (2019) Developmental control of plant Rho GTPase nano-organization by the lipid phosphatidylserine. Science **364**: 57–62

Poraty-Gavra L, Zimmermann P, Haigis S, Bednarek P, Hazak O, Stelmakh OR, Sadot E, Schulze-Lefert P, Gruissem W, Yalovsky S (2013) The Arabidopsis Rho of plants GTPase AtROP6 functions in developmental and pathogen response pathways. Plant Physiol **161**: 1172–1188

Qin L, Zhou Z, Li Q, Zhai C, Liu L, Quilichini TD, Gao P, Kessler SA, Jaillais Y, Datla R, et al. (2020) Specific recruitment of phosphoinositide species to the plant-pathogen interfacial membrane underlies Arabidopsis susceptibility to fungal infection. Plant Cell **32**: 1665–1688

Raffaele S, Mongrand S, Gamas P, Niebel A, Ott T (2007) Genome-wide annotation of remorins, a plant-specific protein family: evolutionary and functional perspectives. Plant Physiol **145**: 593–600

Raffaele S, Bayer E, Lafarge D, Cluzet S, German Retana S, Boubekeur T, Leborgne-Castel N, Carde JP, Lherminier J, Noirot E, et al. (2009) Remorin, a solanaceae protein resident in membrane rafts and plasmodesmata, impairs potato virus X movement. Plant Cell **21**: 1541–1555

Rajendran L, Simons K (2005) Lipid rafts and membrane dynamics. J Cell Sci **118**: 1099–1102

Rausche J, Stenzel I, Stauder R, Fratini M, Trujillo M, Heilmann I, Rosahl S (2020) A phosphoinositide 5-phosphatase from Solanum tuberosum is activated by PAMP-treatment and may antagonize phosphatidylinositol 4,5-bisphosphate at Phytophthora infestans infection sites. New Phytol. DOI: 10.1111/nph.16853

Read SM, Clarke AE, Bacic A (1993) Stimulation of growth of cultured Nicotiana tabacum W 38 pollen tubes by poly(ethylene glycol) and Cu(II) salts. Protoplasma **177**: 1–14

Riedl J, Crevenna AH, Kessenbrock K, Yu JH, Neukirchen D, Bista M, Bradke F, Jenne D, Holak TA, Werb Z, et al. (2008) Lifeact: a versatile marker to visualize F-actin. Nat Methods **5**: 605–607

Rodriguez-Villalon A, Gujas B, van Wijk R, Munnik T, Hardtke CS (2015) Primary root protophloem differentiation requires balanced phosphatidylinositol-4,5-biphosphate levels and systemically affects root branching. Development **142**: 1437–1446

Roy A, Levine TP (2004) Multiple pools of phosphatidylinositol 4-phosphate detected using the pleckstrin homology domain of Osh2p. J Biol Chem **279**: 44683–44689

Saavedra L, Balbi V, Lerche J, Mikami K, Heilmann I, Sommarin M (2011) PIPKs are essential for rhizoid elongation and caulonemal cell development in the moss Physcomitrella patens. Plant J **67**: 635–647

Saavedra L, Catarino R, Heinz T, Heilmann I, Bezanilla M, Malho R (2015) Phosphatase and tensin homolog is a growth repressor of both rhizoid and gametophore development in the moss Physcomitrella patens. Plant Physiol **169**: 2572–2586

Sampathkumar A, Lindeboom JJ, Debolt S, Gutierrez R, Ehrhardt DW, Ketelaar T, Persson S (2011) Live cell imaging reveals structural associations between the actin and microtubule cytoskeleton in Arabidopsis. Plant Cell **23**: 2302–2313

Schindelin J, Arganda-Carreras I, Frise E, Kaynig V, Longair M, Pietzsch T, Preibisch S, Rueden C, Saalfeld S, Schmid B, et al. (2012) Fiji: an open-source platform for biological-image analysis. Nat Methods **9**: 676–682

Sekereš J, Pejchar P, Šantrůček J, Vukašinović N, Žárský V, Potocký M (2017) Analysis of exocyst subunit EXO70 family reveals distinct membrane polar domains in tobacco pollen tubes. Plant Physiol **173**: 1659–1675

Shimada TL, Betsuyaku S, Inada N, Ebine K, Fujimoto M, Uemura T, Takano Y, Fukuda H, Nakano A, Ueda T (2019) Enrichment of phosphatidylinositol 4,5-bisphosphate in the extra-invasive hyphal membrane promotes colletotrichum infection of Arabidopsis thaliana. Plant Cell Physiol **60**: 1514–1524

Simon ML, Platre MP, Marques-Bueno MM, Armengot L, Stanislas T, Bayle V, Caillaud MC, Jaillais Y (2016) A PtdIns(4)P-driven electrostatic field controls cell membrane identity and signalling in plants. Nat Plants **2**: 16089

Simon ML, Platre MP, Assil S, van Wijk R, Chen WY, Chory J, Dreux M, Munnik T, Jaillais Y (2014) A multi-colour/multi-affinity marker set to visualize phosphoinositide dynamics in Arabidopsis. Plant J **77**: 322–337

Simons K, Ikonen E (1997) Functional rafts in cell membranes. Nature **387**: 569–572

Simons K, Toomre D (2000) Lipid rafts and signal transduction. Nat Rev Mol Cell Biol **1**: 31–39

Simons K, Vaz WL (2004) Model systems, lipid rafts, and cell membranes. Annu Rev Biophys Biomol Struct **33**: 269–295

Skirpan AL, Dowd PE, Sijacic P, Jaworski CJ, Gilroy S, Kao TH (2006) Identification and characterization of PiORP1, a Petunia oxysterol-binding-protein related protein involved in receptor-kinase mediated signaling in pollen, and analysis of the ORP gene family in Arabidopsis. Plant Mol Biol **61**: 553–565

Sousa E, Kost B, Malho R (2008) *Arabidopsis* phosphatidylinositol-4-monophosphate 5-kinase 4 regulates pollen tube growth and polarity by modulating membrane recycling. Plant Cell **20**: 3050–3064

Spitzer M, Wildenhain J, Rappsilber J, Tyers M (2014) BoxPlotR: a web tool for generation of box plots. Nat Methods **11**: 121–122

Stanislas T, Hüser A, Barbosa ICR, Kiefer CS, Brackmann K, Pietra S, Gustavsson A, Zourelidou M, Schwechheimer C, Grebe M (2015) Arabidopsis D6PK is a lipid domain-dependent mediator of root epidermal planar polarity. Nature Plants **1**: 15162

Stenzel I, Ischebeck T, Quint M, Heilmann I (2012) Variable regions of PI4P 5-kinases direct PtdIns(4,5)P2 toward alternative regulatory functions in tobacco pollen tubes. Front Plant Sci **2**: 1–14

Stenzel I, Ischebeck T, König S, Holubowska A, Sporysz M, Hause B, Heilmann I (2008) The type B phosphatidylinositol-4-phosphate 5-kinase 3 is essential for root hair formation in *Arabidopsis thaliana*. Plant Cell **20**: 124–141

Sun J, Eklund DM, Montes-Rodriguez A, Kost B (2015) In vivo Rac/Rop localization as well as interaction with RhoGAP and RhoGDI in tobacco pollen tubes: analysis by low-level expression of fluorescent fusion proteins and bimolecular fluorescence complementation. Plant J **84**: 83–98

Synek L, Vukasinovic N, Kulich I, Hala M, Aldorfova K, Fendrych M, Zarsky V (2017) EXO70C2 is a key regulatory factor for optimal tip growth of pollen. Plant Physiol **174**: 223–240

Tamura K, Peterson D, Peterson N, Stecher G, Nei M, Kumar S (2011) MEGA5: molecular evolutionary genetics analysis using maximum likelihood, evolutionary distance, and maximum parsimony methods. Mol Biol Evol **28**: 2731–2739

Tejos R, Sauer M, Vanneste S, Palacios-Gomez M, Li H, Heilmann M, van Wijk R, Vermeer JE, Heilmann I, Munnik T, et al. (2014) Bipolar plasma membrane distribution of phosphoinositides and their requirement for auxin-mediated cell polarity and patterning in Arabidopsis. Plant Cell **26**: 2114–2128

Tinevez J-Y, Perry N, Schindelin J, Hoopes GM, Reynolds GD, Laplantine E, Bednarek SY, Shorte SL, Eliceiri KW (2017) TrackMate: an open and extensible platform for single-particle tracking. Methods **115**: 80–90

Toth K, Stratil TF, Madsen EB, Ye J, Popp C, Antolin-Llovera M, Grossmann C, Jensen ON, Schussler A, Parniske M, et al. (2012) Functional domain analysis of the Remorin protein LjSYMREM1 in Lotus japonicus. PLoS One **7**: e30817

Twell D, Yamaguchi J, McCormick S (1990) Pollen-specific gene expression in transgenic plants: coordinate regulation of two different tomato gene promoters during microsporogenesis. Development **109**: 705–713

van Leeuwen W, Vermeer JE, Gadella, TW Jr Munnik T (2007) Visualization of phosphatidylinositol 4,5-bisphosphate in the plasma membrane of suspension-cultured tobacco BY-2 cells and whole Arabidopsis seedlings. Plant J **52**: 1014–1026

Varnai P, Balla T (1998) Visualization of phosphoinositides that bind pleckstrin homology domains: calcium- and agonist-induced dynamic changes and relationship to *myo*-[^{3}H]inositol-labeled phosphoinositide pools. J Cell Biol **143**: 501–510

Vermeer JE, Thole JM, Goedhart J, Nielsen E, Munnik T, Gadella TW Jr (2009) Imaging phosphatidylinositol 4-phosphate dynamics in living plant cells. Plant J **57**: 356–372

Vidali L, Rounds CM, Hepler PK, Bezanilla M (2009) LifeAct-mEGFP reveals a dynamic apical F-actin network in tip growing plant cells. PLoS One **4**: e5744

Vincent P, Chua M, Nogue F, Fairbrother A, Mekeel H, Xu Y, Allen N, Bibikova TN, Gilroy S, Bankaitis VA (2005) A Sec14p-nodulin domain phosphatidylinositol transfer protein polarizes membrane growth of *Arabidopsis thaliana* root hairs. J Cell Biol **168**: 801–812

Yalovsky S, Bloch D, Sorek N, Kost B (2008) Regulation of membrane trafficking, cytoskeleton dynamics, and cell polarity by ROP/RAC GTPases. Plant Physiol **147**: 1527–1543

Zarza X, Van Wijk R, Shabala L, Hunkeler A, Lefebvre M, Rodriguez-Villalon A, Shabala S, Tiburcio AF, Heilmann I, Munnik T (2020) Lipid kinases PIP5K7 and PIP5K9 are required for polyamine-triggered K(+) efflux in Arabidopsis roots. Plant J **104**: 416–432

Zhang Y, Immink R, Liu CM, Emons AM, Ketelaar T (2013) The Arabidopsis exocyst subunit SEC3A is essential for embryo development and accumulates in transient puncta at the plasma membrane. New Phytol **199**: 74–88

Zhao Y, Yan A, Feijo JA, Furutani M, Takenawa T, Hwang I, Fu Y, Yang Z (2010) Phosphoinositides regulate clathrin-dependent endocytosis at the tip of pollen tubes in Arabidopsis and tobacco. Plant Cell **22**: 4031–4044